Raytheon

NET HEAT FLUX

VISIBLE/INFRARED IMAGER/RADIOMETER SUITE ALGORITHM THEORETICAL BASIS DOCUMENT

Version 5: March 2002

Corinne Carter
Quanhua Liu
Wenli Yang
Dorlisa Hommel

William Emery, Science Team Member
University of Colorado

RAYTHEON SYSTEMS COMPANY
Information Technology and Scientific Services
4400 Forbes Boulevard
Lanham, MD 20706

SBRS Document #: Y2407-NetHeatFlux-ATBD-Rev5

EDR: Net Heat Flux (40.7.5)

Doc No: Y2407
Version: 5
Revision: 0

	FUNCTION	NAME	SIGNATURE	DATE
Prepared By	EDR Developer	C. Carter		1/25/2002
Approved By	Relevant Lead	D. HOMMEL		2/1/02
Approved By	Chief Scientist	S. MILLER		2/8/02
Released By	Algorithm IPT Lead	P. KEALY		2/15/02

TABLE OF CONTENTS

LIST OF FIGURES

LIST OF TABLES

GLOSSARY OF ACRONYMS

6S	Second Simulation of the Satellite Signal in the Solar Spectrum
ATBD	Algorithm Theoretical Basis Document
BSRN	Baseline Surface Radiation Network
CERES	Clouds and the Earth's Radiation Energy System
CMIS	Conical Scanning Microwave Imager/Sounder
COARE	Coupled Ocean-Atmosphere Response Experiment
CrIS	Cross Track Infrared Sounder
DISORT	Discrete Ordinate Radiative Transfer
EDR	Environmental Data Record
ENSO	El Niño/Southern Oscillation
ERBE	Earth Radiation Budget Experiment
IP	Intermediate Product
ISCCP	International Satellite Cloud Climatology Project
IST	Ice Surface Temperature
LOWTRAN	Low Resolution Atmospheric Radiance and Transmittance Model
MODTRAN	Moderate Resolution Atmospheric Radiance and Transmittance Model
NCAR	National Center for Atmospheric Research
NCEP	National Centers for Environmental Prediction
NHF	Net Heat Flux
NPOESS	National Polar-orbiting Operational Environmental Satellite System
SSM/I	Special Sensor Microwave/Imager
TBD	To Be Determined
TBR	To Be Reviewed
TOGA	Tropical Ocean Global Atmosphere
TOVS	TIROS Operational Vertical Sounder
VIIRS	Visible/Infrared Image Radiometer Suite
WCRP	World Climate Research Program

ABSTRACT

For the first time, the Net Heat Flux (NHF) Environmental Data Record (EDR) is being developed as an operational product derived from satellite measurements. NHF can be derived from the National-Orbiting Operational Environmental Satellite System (NPOESS), a multisensor satellite system. Sea surface temperature and shortwave radiation flux can be obtained from the Visible/Infrared Image Radiometer Suite (VIIRS). Profiles of atmospheric temperature and humidity can be derived from Cross- track Infrared Sounder (CrIS) or Conical Scanning Microwave Imager/ Sounder (CMIS) data, and sea surface wind speed can be estimated from CMIS data. Because CMIS data can be used for both clear and cloudy conditions, the algorithms can also be used for cloudy conditions. However, the current requirements for the Net Heat Flux EDR specify that it must only be produced under clear- sky conditions, but during both daytime and nighttime.

NHF contains two radiative flux components (net shortwave and longwave radiation at the surface) and two turbulent (sensible and latent) heat flux components. These components are used widely for studying the greenhouse effect, interaction between ocean and atmosphere, and the global water cycle. They are key parameters for developing ocean and atmospheric models. NHF, however, is neither well understood nor easy to validate due to the sparse in-situ measurements and large measurement uncertainties. Even with modern techniques and sophisticated design, it is difficult to achieve an accuracy of 5 Wm^{-2} for each NHF component.

Our present formulas for calculating sensible and latent heat fluxes are approximations based on experimental evidence. So far, comparisons are only made to model simulations due to a lack of in-situ measurements. The threshold requirement for accuracy, but not for precision, has been achieved. Although the NHF uncertainty is 25 Wm^{-2}, it is still useful in determining the bulk temperature of the sea surface, ocean current, and for ocean-atmospheric modeling, especially for climate study. It may achieve the threshold requirements if uncertainties of non-VIIRS data are not or only partially considered.

In order to improve the retrieval accuracy for the air temperature and surface specific humidity, an optimized algorithm for CrIS data from the boundary layer is being developed.

1.0 INTRODUCTION

1.1 PURPOSE

Net heat flux over the oceans is one of the key parameters governing the atmosphere-ocean interaction. It is required for weather prediction and climate studies related to the global energy and water cycles. Using suitable models, net heat flux can be used to reproduce and predict variations of the global hydrological regime and its impact on atmospheric and surface dynamics, as well as variations in regional hydrological processes and water resources and responses to such environmental changes as the increase in greenhouse gas forcing. Net heat flux, which depends on clouds, sea surface temperature, and sea surface wind, is an important component of atmosphere-ocean interactions such as the El Niño/Southern Oscillation (ENSO) phenomenon. Another atmosphere-ocean interaction may act to set an upper bound to sea surface temperatures. In the upper range of sea surface temperatures, the greenhouse effect increases dramatically with surface temperature as the specific humidity of the atmosphere increases. In response to this "super greenhouse effect," highly reflective cirrus clouds are produced; these clouds act like a thermostat, shielding the ocean from solar radiation (Ramanathan and Collins, 1991). The cirrus clouds reduce solar radiation, but have little effect on outgoing longwave radiation due to their low temperature; this causes a deficit of radiation at the surface. The effect may limit sea surface temperature to less than 305 K.

The net heat flux is composed of latent and sensible heat fluxes, combined with short-wave and long-wave radiation fluxes at the surface in both upward and downward directions. Each component has significance for weather prediction and the study of our environment. Long-wave radiation relates to forcing by greenhouse gases, such as carbon dioxide. Net short-wave radiation is altered by the variation of aerosols and surface albedo. Sensible heat flux is directly dependent on changes in the sea surface temperature, and latent heat flux is a measurement of evaporation. It has been suggested that evaporation from the ocean is a mechanism responsible for changes in the sea surface temperature. The capacity of the atmosphere to hold water vapor is much greater at high temperatures than at low ones (Liu and Zhang, 1994), since the saturation pressure of water vapor is an exponential function of temperature. The latent heat needed for evaporation cools the ocean and provides a negative feedback (Priestley, 1966).

An atlas of the heat flux has been produced for the global monthly mean with a spatial resolution of 4 degrees by 5 degrees (see Figures 1-5, Oregon St. CRI Global Ocean Heat Flux). The maximum sensible heat flux is generally found over the warm waters of the Kuroshio Current and the Gulf Stream. The sensible heat flux is maximized during cold-air outbreaks due to large humidity differences coupled with strong offshore winds (Agee and Howley, 1977). The large positive net heat flux in the tropical region is due to the large solar incident radiation there. The net heat flux in high latitudes is negative because of the low solar radiation.

Retrieval of a Net Heat Flux Environmental Data Record (EDR) from NPOESS depends on data or EDRs from many NPOESS sensors, including the Visible/Infrared Image Radiometer Suite (VIIRS), Conical Scanning Microwave Imager/Sounder (CMIS), and Cross Track Infrared Sounder (CrIS). The methods for obtaining net heat flux described in this document require the use of different combinations of data from different instruments for each component. The shortwave radiation flux at the surface is directly calculated from VIIRS radiances. The

longwave net radiation flux over the oceans may be calculated from VIIRS sea surface temperatures and CrIS atmospheric profiles, or CMIS brightness temperatures. Latent and sensible heat fluxes are calculated from the sea surface wind, air temperature and surface specific humidity, which are EDRs of CMIS and CrIS. In the derivation of CrIS EDRs, the three-dimensional effect of clouds must be considered in the microwave radiative transfer (Haferman *et al*., 1996).]

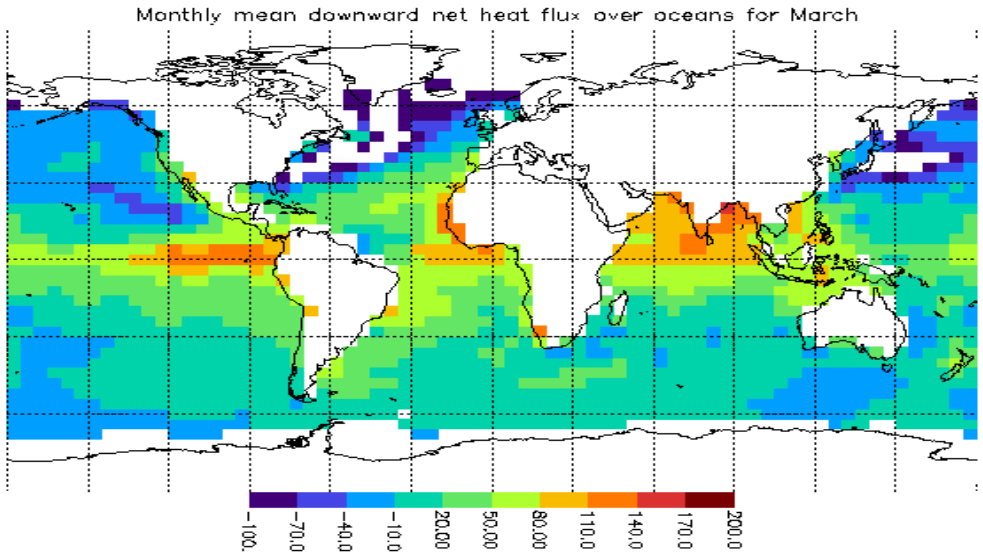

Figure 1. Monthly mean net heat flux (unit: Wm^{-2}), produced from the dataset of Oregon St. CRI Global Ocean Heat Flux.

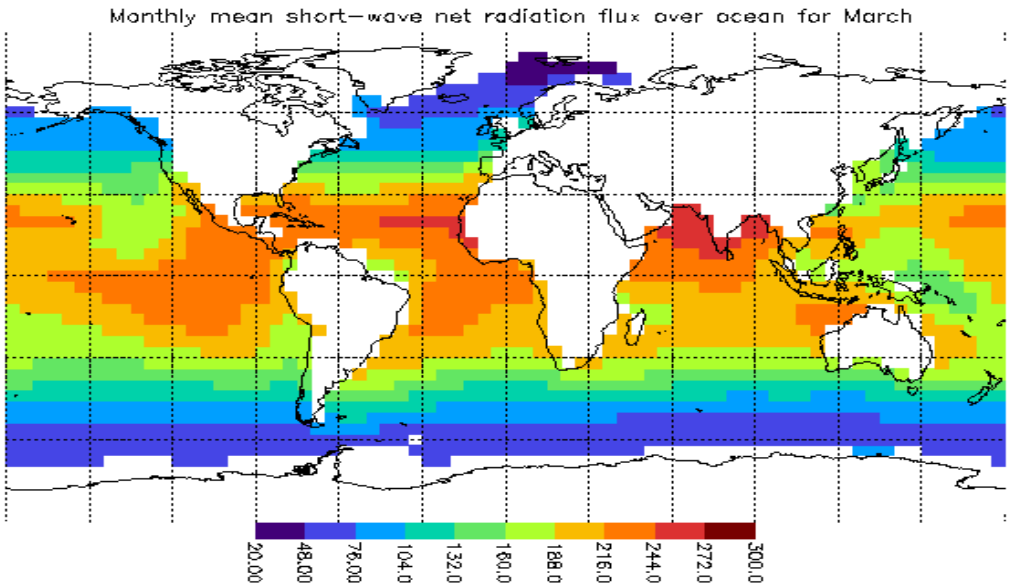

Figure 2. Monthly mean short-wave net radiation flux over oceans (unit: Wm^{-2}), produced from the dataset of Oregon St. CRI Global Ocean Heat Flux.

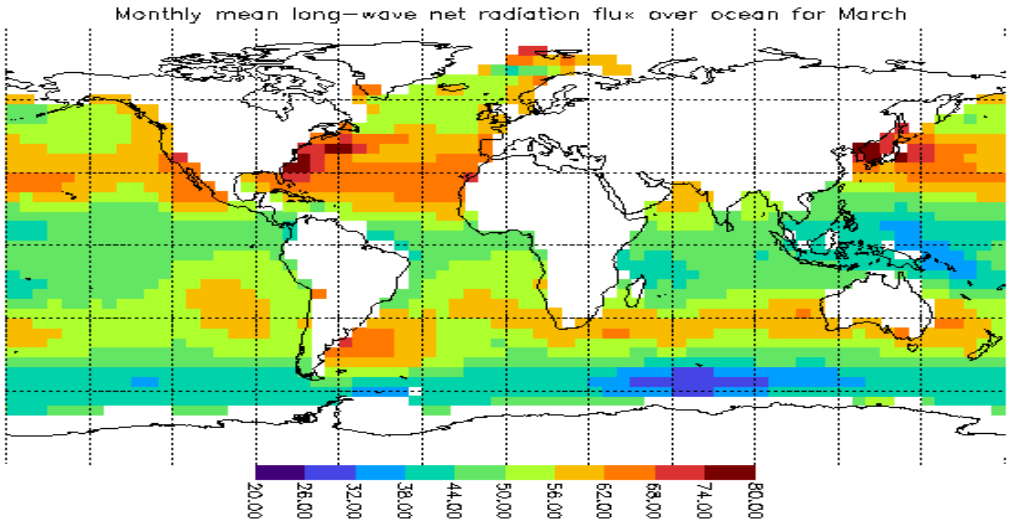

Figure 3. Monthly mean long-wave net radiation flux over oceans (unit: Wm^{-2}), produced from the dataset of Oregon St. CRI Global Ocean Heat Flux.

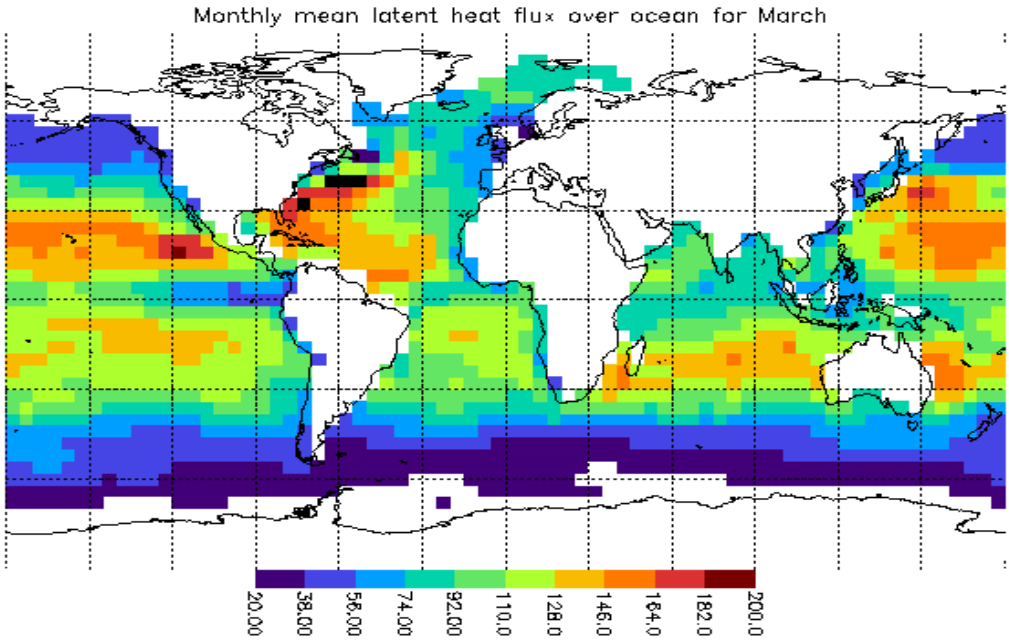

Figure 4. Monthly mean latent heat flux over oceans (unit: Wm^{-2}), produced from the dataset of Oregon St. CRI Global Ocean Heat Flux.

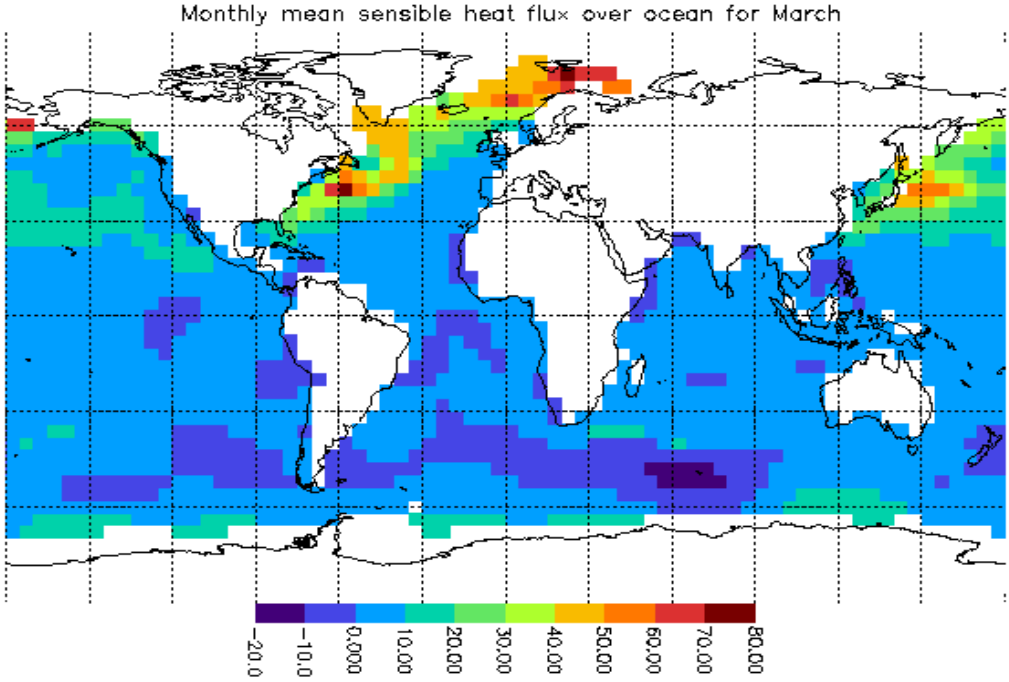

Figure 5. Monthly mean sensible heat flux over oceans (unit: Wm^{-2}), produced from the dataset of Oregon St. CRI Global Ocean Heat Flux.

1.2 SCOPE

This Algorithm Theoretical Basis Document (ATBD) describes the theoretical basis of the VIIRS Net Heat Flux (NHF) algorithm. Section 1 describes the purpose and scope of this document. Section 2 is an overview, of previous work, present research, and future perspective. Present and potential applications of the methods described in Section 2 to the VIIRS system are detailed in Section 3, "Algorithm Description." Section 3 also provides useful physical background, mathematical treatment information, and sensitivity tests that help in selecting valuable variables and determining retrieval accuracies. A functional flowdown shows the main structure of the retrieval algorithm for each component of the net heat flux. The statistical results represent algorithm validation and assessment of the sensor abilities.

1.3 VIIRS REQUIREMENTS

The National Polar-orbiting Operational Environmental Satellite System (NPOESS) science team for daily and nighttime 20 km ocean products (VIIRS, 1997) proposed the Net Heat Flux EDR. Required at first for both clear and cloudy cases, it was later required for clear conditions only. The Net Heat Flux EDR requirements from the VIIRS Sensor Requirements Document *[Y-1]* are provided in Table 1. From these requirements and information about the VIIRS instrument in development, new EDR requirements were derived by Raytheon. These derived requirements, including thresholds, objectives, and specifications, are displayed in Table 1.

Table 1. NHF EDR requirement (derived).

Parameter No.		Thresholds	Objectives	Specifications
V40.7.5-1	a. Horizontal Cell Size	20 km	5 km	20 km
V40.7.5-2	b. Horizontal Reporting Interval	20 km	5 km	20 km
V40.7.5-3	c. Horizontal Coverage	Oceans	Oceans	Oceans
V40.7.5-4	d. Measurement Range	-1000 to 1000 Wm^{-2}	-2000 to 2000 Wm^{-2}	-2000 to 2000 Wm^{-2}
V40.7.5-5	e. Measurement Accuracy	10 Wm^{-2}	1 Wm^{-2}	15 Wm^{-2}
V40.7.5-6	f. Measurement Precision	5 Wm^{-2} (25)*	1 Wm^{-2} (10)*	25 Wm^{-2}
V40.7.5-7	g. Mapping Uncertainty	7 km	1 km	7 km
	h. Maximum Local Average Revisit Time	6 hours	3 hours	6 hours
	i. Maximum Local Refresh	6 hours	3 hours	6 hours
V40.7.5-8	j. Minimum Swath Width	1700 km	3000 km	1700 km
*Recommended				

1.4 REVISIONS

This is the fifth version of this document, dated January 2002. Changes are made to the text to reflect the selection of the method to be used in calculating longwave and latent heat fluxes. In both cases, VIIRS SST data will be used along with CrIS atmospheric profiles. Other changes have been made to the algorithms. The look-up table for longwave radiation will be derived from MODTRAN. CMIS wind speeds will be used in the shortwave flux algorithm to derive values for sea surface albedo. The shortwave flux can be calculated from a look-up table of MODTRAN-derived or empirical coefficients. These changes are reflected in the text and figures of Section 3.

For the fourth version of this document, dated May 2001, additions were made to the VIIRS Data section.

The third version was dated May 2000. For the third version the rationale for proposing the new EDR requirements contained in Table 1 was provided as follows: The change of the Minimum Swath Width from 3000 km to 1700 km is due to the smaller swath width of CMIS; The sea surface wind from CMIS' EDR is required for calculating both the latent and sensible heat flux; Simultaneous VIIRS and CMIS measurements are required because the sea surface wind can change rapidly; the low limit of the Measurement Range is extended to –1000 (Threshold) and –2000 Wm^{-2} (Objective) because the Net Heat Flux is usually negative at nighttime.

2.0 OVERVIEW

Net heat flux was proposed as an operational satellite product for the first time by the VIIRS science team. Its four components challenge NPOESS sensors as well as retrieval algorithms. Direct measurements of these parameters are very sparse. Current state-of-the art latent heat flux measurements from buoys achieve an accuracy of only 0-20 Wm^{-2}, whereas studies show that current satellite measurements of latent heat flux cannot be obtained to much better than 40 Wm^{-2}. For single matchups (instantaneous), the standard deviation of the latent heat flux between ship and satellite measurements is about 30 Wm^{-2} (Schluessel, 1996).

Satellite remote sensing has been shown to be a viable method for retrieval of net heat flux, although the potential uncertainties are great. Curry et al. (1999) have studied satellite- measured surface heat flux in detail. They use a high-resolution dataset from the Tropical Ocean Global Atmosphere Coupled Ocean-Atmosphere Response Experiment (TOGA COARE) with a spatial resolution of 50 km and temporal resolution of 3h. In-situ comparison between satellite-derived and TOGA measured short-wave and long-wave net radiation as well as latent and sensible heat flux (Curry et al. (1999)) shows a large uncertainty in calculating the surface short-wave net radiation, long-wave net radiation, latent heat flux, and sensible heat flux for three-hourly values (see Table 2).

The error calculated from instantaneous comparisons between surface and satellite- derived longwave and shortwave radiation fluxes at the surface are generally so large that only monthly mean satellite data are are reported. The error of the monthly averaged net radiation flux at the surface is about 10 Wm^{-2} (Darnell *et al*., 1992; Gupta *et al*., 1992; or see http://agni.larc.nasa.gov /model_doc.html).

The satellite retrieval of sensible and latent heat flux depends critically on the estimation of sea surface temperature, sea surface wind, and surface humidity. The present accuracy of 0.5 K for sea surface temperature is insufficient to meet the VIIRS requirements for NHF. In addition, the skin temperature as measured by the satellite is typically a few tenths of a degree cooler than the bulk temperature (Robinson *et al*., 1984), but can be up to 1 K cooler or warmer in extreme circumstances; this is the so-called “skin effect.” Sea surface wind can also affect sea surface temperature retrieval from space. Sea surface wind speed is generally calculated from the microwave sensors such as the Special Sensor Microwave/Imager (SSM/I) (Liu *et al*., 1997). The water emissivity can change with sea surface roughness due to sea surface wind (Harris *et al*., 1994). The emissivity of the sea surface changes significantly above viewing zenith angles of about 50^{o}. Turbulent heat transfer is almost a linear function of sea surface wind; errors of ten percent in the retrieval of sea surface wind are the best current research results. A 10 percent (or about 1 ms^{-1}) error in sea surface wind can result in an error of 10 Wm^{-2} in NHF due to the error introduced in the calculation of sensible and latent heat fluxes.

For purposes of deriving turbulent fluxes using the NPOESS system, low- level air temperature and surface humidity may be obtained from the atmospheric profiles of CrIS or CMIS or analysis from a numerical forecast model. Unfortunately, their accuracy is unlikely to be better than 10 percent in near the future, which is far beyond the NHF requirement. Retrieval accuracy for net heat flux is also affected by atmospheric correction, foam, atmospheric stability, and wind direction. Knowledge of the roughness spectrum of the ocean would be very helpful. One of the

NPOESS sensors, CMIS, should be able to derive the sea surface wind speed and direction. Its prototype, "Windsat," is under development.

Table 2. Comparison of the surface short-wave net radiation, long-wave net radiation, latent heat flux, and sensible heat flux for three-hourly values between ship measurements and calculations using satellite data (adopted from Curry et al. 1999, unit: W m^{-2}).

	Net short-wave flux	Net long-wave flux	Latent heat flux	Sensible heat flux
Bias (ship-satellite)	-26	-8	19	-4
Rms error	86	16	45	11
Correlation	0.96	0.35	0.72	0.37

2.1 BACKGROUND

Net heat flux can only be obtained by combining data from multiple sensors. Schmetz (1989) has reviewed methods for obtaining the surface radiation fluxes. The net longwave radiation over the ocean has been retrieved using different formulas, and the performances of these formulas have been evaluated. Bulk formulas for longwave net radiation over the ocean surface (Anderson, 1952) calculate the longwave net radiation at the sea surface from measured sea surface temperature, air temperature, humidity of the boundary layer, and cloud cover. Gilman and Carrett (1994) discussed eight bulk formulas and found that the resulting annual mean difference of the longwave net radiation over the Mediterranean Sea can be up to 20 Wm^{-2}. Gupta (1989) used the International Satellite Cloud Climatology Project (ISCCP) data set to determine the longwave net radiation at the surface. The main inputs of the Gupta (1999) algorithm are surface temperature and emissivity, atmospheric profiles of temperature and humidity, fractional cloud amounts, and cloud heights.

The Gupta (1989) algorithm is flexible and therefore adaptable in using input data from a wide variety of sources. This algorithm is based on parameterized equations developed expressly for computing surface longwave radiation in terms of meteorological parameters, which are available from satellite data/or other operational sources. Also, these equations are based secondarily on the physics of radiative transfer, as they were developed from a large database of surface fluxes computed with an accurate, narrow-band radiative transfer model. Zhi and Harshvardhan (1993) calculated the longwave net radiation from a combination of general circulation model cloud radiative forcing fields, cloud radiative forcing at the top of the atmosphere from ERBE (Earth Radiation Budget Experiment), TOVS (TIROS Operational Vertical Sounder) profiles, and sea surface temperatures of ISCCP C1 data. The longwave net radiation (Smith and Woolf, 1983) over oceans also can be derived from a microwave sensor, such as SSM/I.

For shortwave radiation, a statistical relationship between the reflected radiation field at the top of the atmosphere and at the surface often is applied. This relationship is affected by the solar zenith angle, gaseous and aerosol absorption and scattering, and surface reflectivity. Because atmospheric constituents absorb and scatter, but do not emit radiation at solar wavelengths, there

is a coupling between the radiation fields at the top and at the surface (Schmetz, 1989). The character of the coupling depends on the absorption within the atmosphere. In contrast to the strong variability of the radiation budget at the top of the atmosphere and at the surface, atmospheric absorption remains relatively stable. However, small changes in the magnitude of the atmospheric absorption are correlated with changes in the reflected shortwave flux at the top of the atmosphere (Li *et al*., 1993).

Darnell and Staylor (1988) developed another approach for calculating the surface shortwave radiation. The basic idea of this approach is that the surface solar radiation is approximately a product of sun irradiance at the top of the atmosphere and the "effective transmission." The effective transmission is a resultant optical depth arising from all absorption and scattering processes acting on the vertical radiation. Individual, well-developed vertical optical depth models are available to represent most of these atmospheric scattering and absorption processes. The optical depths of these separate components are generally either small or spectrally nonoverlapping. The effective transmission is a function of water vapor, ozone, carbon dioxide, oxygen, molecular scattering, surface albedo effects, and aerosol effects. The Li et al (1993) and Darnell and Staylor (1988) algorithms were developed based on radiation flux at the top of the atmosphere, where the radiation flux is either from ERBE measurements or calculated from narrow band radiances.

There are four standard techniques for measuring sensible and latent heat fluxes (Chou, 1993): (a) eddy correlation; (b) inertial subrange dissipation; (c) mean profiles; and (d) bulk aerodynamic methods (e.g., Paulson *et al*., 1972; Kondo, 1975; Garratt, 1977, Large and Pond, 1981; Blanc, 1987). Only the eddy correlation method is a direct measure of the fluxes. It requires time series' of vertical wind, horizontal wind, and temperature and humidity fluctuations. The measurement of vertical wind requires a rigid, slender supporting structure to avoid contamination due to motion and flow distortion of the supporting structure. The inertial subrange dissipation method estimates fluxes from the budget equations and the dissipation of turbulent kinetic energy, temperature, and humidity variances. The dissipation variables are determined from the spectra of wind, temperature, and humidity in the inertial subrange. The subrange occurs at frequencies higher than those of dominant ocean waves and ship or buoy motions. Thus the dissipation method is relatively insensitive to platform motions. After verification, this method can be applied to a larger range of experimental sites and conditions as compared to the eddy correlation method. The flux-profile relationships describe relations between the surface fluxes and the mean profiles (gradients) of wind, temperature, and humidity in the atmospheric surface layer. Flux measurements by the profile and dissipation methods are based on these relationships.

For sensible heat flux and latent heat flux, the bulk formula is often used (Chou *et al.*, 1995) because of its extensive use in numerical models and its applicability to a large scale of climatological data sets from ship or buoys or from satellite measurement (Crewell *et al*., 1991). The greatest difficulty in deriving bulk sensible and latent fluxes from space is that the measured radiance is not sensitive to air temperature and surface humidity. The bulk coefficient (Budyko, 1974) is also an empirical coefficient, and is not well known. The development of a reliable bulk scheme, based on direct eddy-correlation measurements, is essential (Isemer and Hasse, 1985).

2.2 VIIRS INSTRUMENT REQUIREMENTS AND CALIBRATION

The VIIRS Net Heat Flux EDR is calculated from absolute VIIRS radiances, other VIIRS EDRs, and data from non-VIIRS NPOESS instruments. Absolute VIIRS radiances are needed to calculate the downwelling shortwave radiation flux at the surface. To calculate the solar radiation flux at the surface, spectral bands, which relate to molecular scattering, aerosol scattering, water vapor and ozone absorption, are required. The sensible and latent components of NHF are derived from non- VIIRS atmospheric profiles in combination with the VIIRS SST and IST EDRs, so they do not drive VIIRS sensor models.

Several sensor noise models have been constructed, with model 0 representing a perfect sensor, and sensor performance progressively degrading as model number increases. It can be seen from Figure 6 that sensor model 3 or better satisfies the EDR requirement for precision, where results are derived based on the baseline set of wavelengths. This sensor model was used for flowdown of the sensor design. The final VIIRS model is better than the sensor model 3.

The required VIIRS wavelengths and bandwidths are provided in Table 3. The direct derivation of the downwelling short-wave radiation flux may relax the requirement on other EDRs such as the aerosols and ozone as well as the humidity profile. The short-wave radiation flux at the top of the atmosphere, which is calculated from the baseline sensor design, can satisfy the EDR requirements. However, the baseline sensor long-wave radiation at the top of the atmosphere and at the surface indicates that the threshold value of 5 Wm^{-2} cannot be satisfied, even if a perfect (noise-free) sensor is used. This is due to the fact that two infrared window channels contain only very coarse and weak information on the vertical distributions of the temperature and humidity. Therefore, the channel M14 ($8.40 - 8.70\ \mu m$) is needed to meet the NHF EDR requirement. Using M14 and two infrared window channels of the baseline, the derived longwave radiation flux at the top of the atmosphere can meet the EDR requirement (see Figure 7).

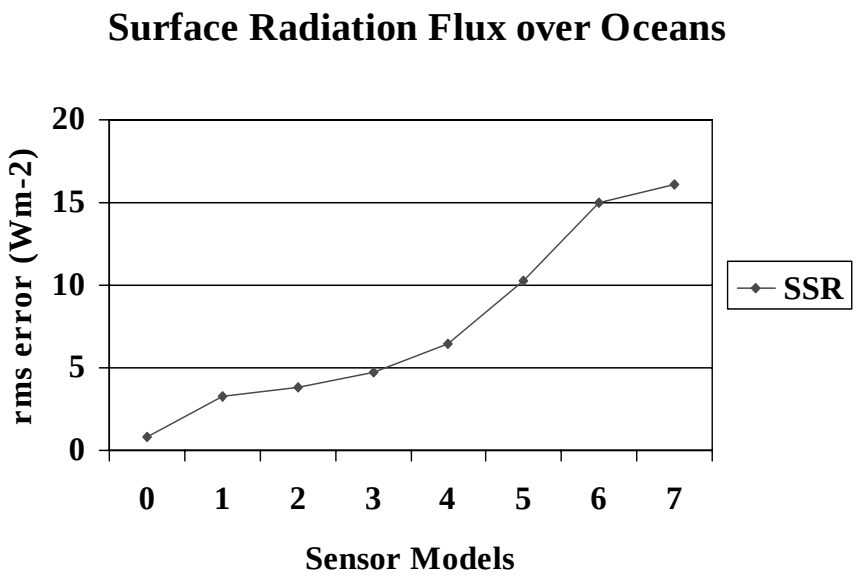

SSR: Surface Shortwave Radiation Flux

Figure 6. Retrieval errors for different sensor models. Sensor model 0 means a perfect sensor.

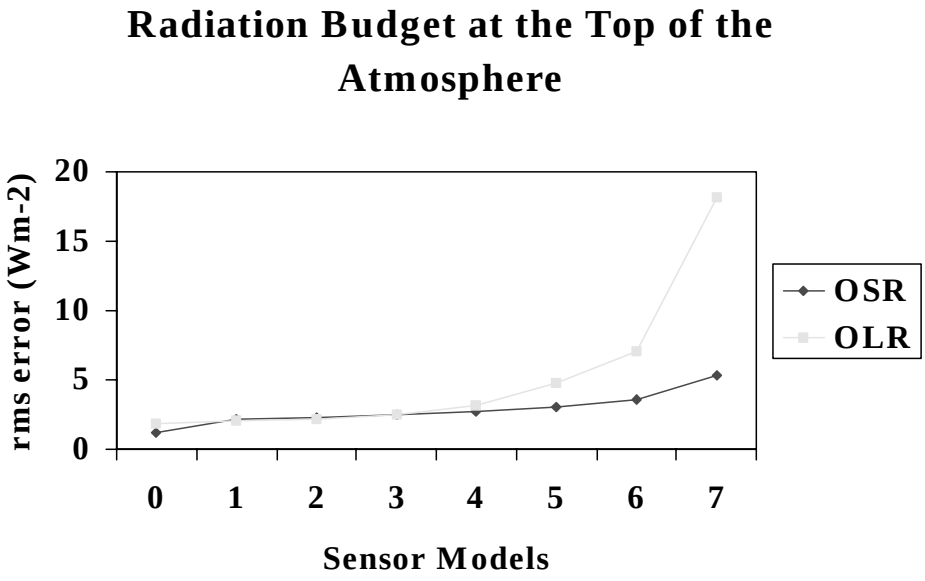

OSR: outgoing shortwave radiation, OLR: outgoing longwave radiation

Figure 7. Retrieval errors for the radiation flux at the top of the atmosphere for different sensor models.

Table 3. VIIRS wavelengths and bandwidths requirements.

1	2	3	4	5	6	7	8	9	10	SST 4	11	12
0.402-0.422	0.435-0.455	0.478-0.498	0.545-0.565	0.662-0.682	0.739-0.754	0.845-0.884	1.371-1.386	1.580-1.640	2.225-2.275	8.40-8.70	10.26-11.26	11.54-12.49

Absolute calibration is required for calculating the shortwave and longwave radiation fluxes, and calibration errors have not been considered. For shortwave radiation, a calibration error of less than 0.5 percent is required, but this is unrealistic considering cost and existing technology. One may use more precise radiation budget measurements from other instruments, such as CERES to adjust VIIRS-derived radiation fluxes at the top of the atmosphere. Then the downward shortwave radiation can be calibrated by using the relationship between the top and surface.

Ssurface-based calibration is another way to maintain a highly accurate calibration. However, such surface-based calibration depends on a radiative transfer code and knowledge of atmospheric conditions. The retrieval accuracy of the longwave net radiation at the surface can meet the NPOESS requirements provided that CMIS' NEdT is less than 0.5 K. The use of microwave radiance or brightness temperatures from CMIS at 6.8, 10.7, 19.35, 22.235, 37, 85.5 GHz and other channels at 60 GHz and 183 GHz would be beneficial. The brightness temperature at 6.8 GHz is sensitive to sea surface temperature. The brightness temperatures at 10.7 and 19.35 GHz should be optimal for determining sea surface wind. Channels 19.35, 22.235, 37, 85.5 GHz have been used in many applications.

3.0 ALGORITHM DESCRIPTION

The Net Heat Flux EDR is a measurement of energy balance over the oceans. This energy balance has been described by radiative transfer theory and turbulence theory. An important constraint for the surface flux is the conservation of total energy. The equation for the heat budget of an interfacial layer is fairly complex because many energy transfers and transformations from one form of energy to another have to be taken into account. These processes take place continuously both at and near the ocean's surface. Most of the transformations start with the absorption of solar radiation and end with the loss of infrared radiation to space. The complete energy cycle is described as follows:

The absorbed solar radiation leads to an increase in the heat content of ocean mixed layer. This thermal energy may, in turn, lead to an upward transfer of sensible, latent, and longwave radiation energy into the atmosphere and a downward transfer of heat into the ocean below the mixed layer. Therefore, turbulent theory is applied to determine the bulk coefficients used in the calculation of sensible and latent heat fluxes. A detailed discussion of the theory of sensible and latent heat transfer within the atmospheric boundary layer can be found in Brutsaert (1982). Refer to Section 3.3.2.5 [TBR] for a more detailed description of the derivation and use of the bulk coefficients for calculating sensible and latent heat fluxes for the VIIRS NHF EDR.

The physics of the interaction of shortwave and longwave radiation with the atmosphere can be described by radiative transfer theory. Much can be found about radiative transfer theory in the literature, including polarized and nonpolarized problems. There are one-dimensional, two-dimensional, and three-dimensional radiative transport theories. Even for one-dimensional radiative transfer, two-stream, successive orders of scattering and the matrix operator method are often applied. As for spectral resolutions, there are line-by-line models, the Moderate Resolution Atmospheric Radiance and Transmittance Model (MODTRAN), the Low Resolution Atmospheric Radiance and Transmittance Model (LOWTRAN), and narrow-band models.

For shortwave radiation, the solar incident radiation flux at the top of the atmosphere is a sum of the shortwave net radiation at the surface, absorbed radiation by the atmosphere, and the reflected radiation flux at the top of the atmosphere. The surface albedo, or fraction of incident shortwave radiation at the surface that is reflected, is also a significant control on net shortwave radiation at the surface. For clear sky cases, the reflected shortwave radiation flux at the top of the atmosphere has a good correlation with the part absorbed by the atmosphere. Thus, it is reasonable to assume a linear relationship between the satellite-measured radiance and the shortwave net radiation over the ocean surface. A second simulation of the satellite signal in the solar spectrum (6S) has been applied to simulate the shortwave radiation flux at surface and satellite-borne VIIRS radiances. The 6S code (Vermote *et al.*, 1997) enables simulation of plane-parallel conditions, taking into account elevated targets and non-lambertian surface boundary conditions. New gases (CH4, N2O, CO) have been integrated into computation of the gaseous transmission.

The selection of 6S or MODTRAN has no influence on the logic of the algorithm. However, it is preferable to base the shortwave retrievals on MODTRAN, since it is complex but versatile, with many successful applications. MODTRAN also models the absorption of radiation by gases in the atmosphere more accurately. MODTRAN 3.7 has 1/cm spectral resolution in the visible and

infrared regions and 5/cm in the ultraviolet area. Two-stream and DISORT (Discrete Ordinate Radiative Transfer) are available in the code. MODTRAN is faster than line-by-line models, but it is not fast enough for large- scale simulations, so it will be used to create look- up tables for use in the shortwave and longwave flux calculations. More information about MODTRAN is available on the World Wide Web at http://www.ontar.com/prod/PcModWin.htm

Derivation of the longwave net radiation is difficult because the atmosphere and surface emit longwave radiation separately. There is no clear correlation between the longwave radiation at the surface and at the top of the atmosphere. MODTRAN version 3.7 code has been used to simulate the longwave net radiation over the oceans and the VIIRS radiance. The results of these MODTRAN simulations are combined with surface temperature and atmospheric profile information to obtain net longwave flux at the surface.

CMIS wind speeds are used in the derivation of surface albedo for the shortwave radiation flux calculation. It is also possible to use CMIS data in the derivation of longwave and latent heat fluxes, but this approach is not the one described in the VIIRS Net Heat Flux Detailed Design *[Y-3230]*. To simulate CMIS microwave brightness temperatures, polarization must be considered. The matrix operator method is one of the commonly used methods, which accounts for scattering and polarization. For a homogeneous layer, the matrix operator method solves the radiative transfer equation in analytical matrices. The solution of the radiative transfer equation for the vertically inhomogeneous atmosphere is obtained recurrently from the analytical solutions for a set of homogeneous layers, where the vertically inhomogeneous atmosphere is subdivided into a set of homogeneous layers (Liu and Ruprecht, 1996).

3.1 PROCESSING OUTLINE

The four components—longwave radiation, shortwave radiation, sensible heat fluxes, and latent heat fluxes—are calculated separately. The longwave net radiation flux, L_{net}, will be calculated from atmospheric profiles from CrIS EDRs and the VIIRS sea surface temperature EDR. In Figure 8, a regression technique is applied to calculate L_{net} from the sea surface temperature and temperature and humidity profiles of the atmosphere. Shortwave net radiation, S_{net}, (see Figure 9) over the oceans can be calculated directly from the VIIRS radiances. The retrieved S_{net} be compared with the surface truth or with the reflected shortwave radiation flux at the top of the atmosphere through an empirical equation is recommended. Sensible, H, and latent, E, heat fluxes can also be calculated (see Figures 10 and 11) from sea surface temperature from VIIRS, and air temperature and surface humidity interpolated from CrIS' temperature and humidity profiles. Bulk formulas are applied, in which bulk coefficients are dependent on the sea surface wind and temperature difference between air and ocean.

Since S_{net} is dependent only on VIIRS radiances, an independent value can be calculated for each VIIRS pixel and then aggregated into 20 km cells. The other components of NHF depend on CrIS profiles along with VIIRS surface temperature information, so input information from both sources is aggregated to the 20 km cells before the flux calculations are performed. If a grid cell is mixed water and ice, longwave and turbulent fluxes will be calculated separately for water and ice, then combined in a weighted average according to the fraction of valid pixels within the cell that are ice.

3.2 ALGORITHM INPUT

3.2.1 VIIRS Data

Information from the VIIRS Cloud Mask IP, VIIRS radiances from the reflective bands in Table 3, and the VIIRS Surface Albedo EDR, are used to calculate the shortwave net radiation flux over the ocean surface. VIIRS sea surface temperatures and ice surface temperatures from the SST and IST EDRs are used in the calculation of longwave, sensible, and latent heat fluxes.

3.2.2 Non-VIIRS Data

Temperature and humidity profiles derived from CrIS are inputs to Net Heat Flux. Sea surface wind calculated from CMIS is an input for Net Heat Flux as well. Atmospheric profile data and surface winds from NCEP are used when CMIS or CrIS data are unavailable. The coefficients needed to convert VIIRS radiances to values of net shortwave radiation at the surface are held in a look- up table, with parameters shown in Table 4 below.

Table 4. Look-up Table Parameters for Deriving Short-Wave Radiation at the Surface.

Parameter	Definition
Wavelength of VIIRS band	The input wavelengths are for VIIRS bands having wavelength less than 3700 nm.
Surface pressure	The look-up table can be generated at the surface pressure of 1013.25 hPa, a standard pressure.
Sea Surface Wind Speed	10 m/s at 10 meters above the sea surface.
Solar zenith angle	16 Gauss discrete angles, which covers 0 to about 85 degrees.
Viewing zenith angle	16 Gauss discrete angles, which covers 0 to 85 degrees.
Relative azimuth angle (solar/viewing)	Every 10 degrees beginning from 0.
Aerosol types	Maritime, coastal, continental, and urban aerosols have 10 optical thicknesses at 555 nm between 0.05 and 3.
Ozone Amount	Ozone amount at 100, 200, 300, 400, and 500 Dobson Unit.
Atmospheric profiles	At least six standard atmospheric profiles.
Ice Surface Albedo	At values of 0.6, 0.8, and 1.

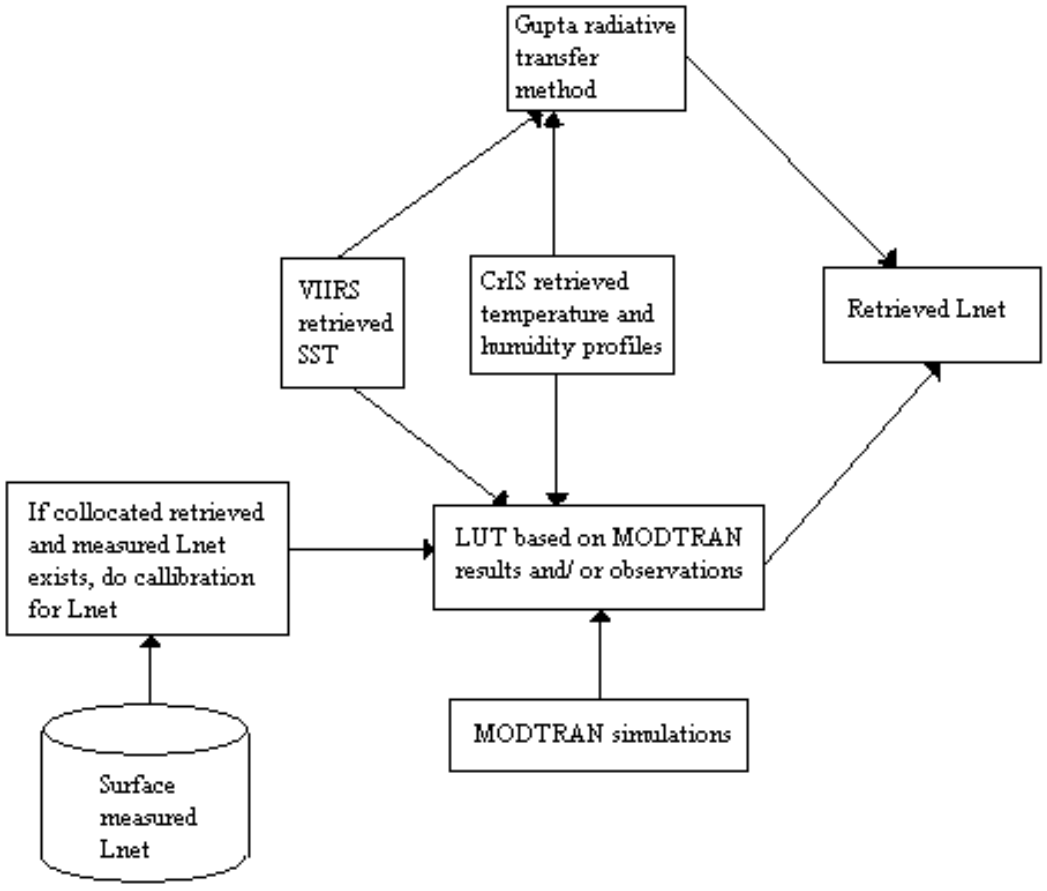

Figure 8. EDR flowdown process diagram for L_{net} .

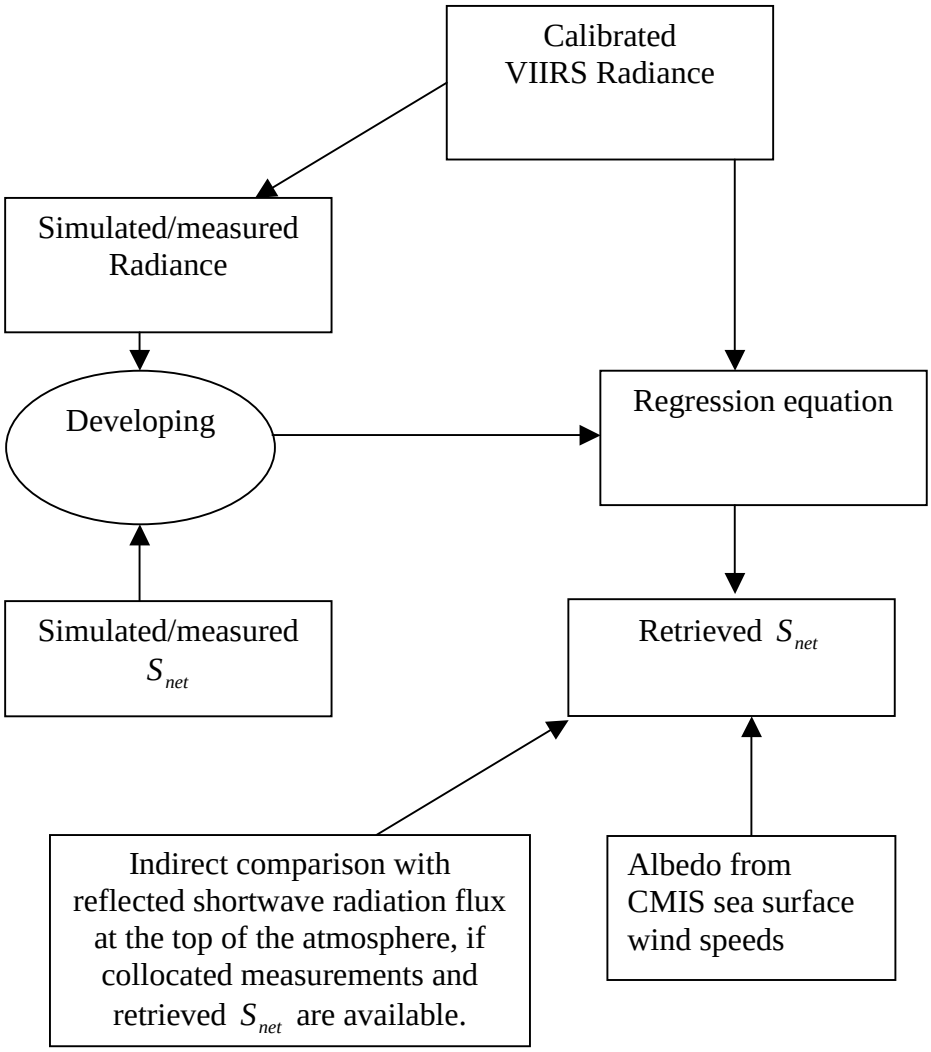

Figure 9. EDR flowdown process diagram for S_{net} .

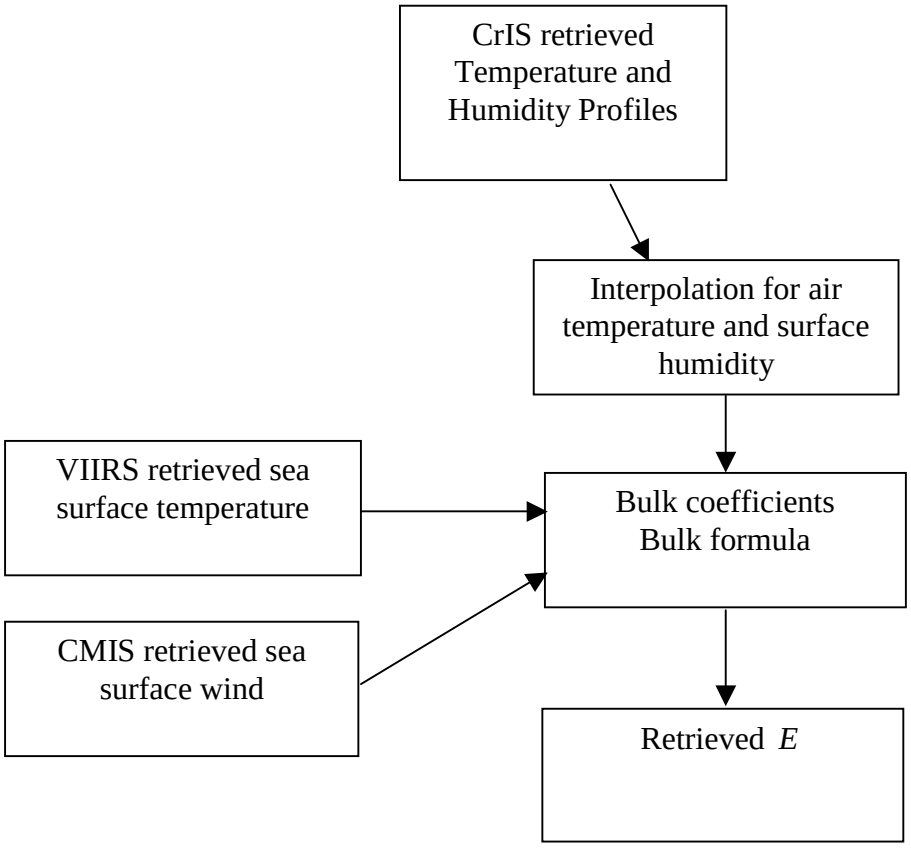

Figure 10. EDR flowdown process for latent heat flux.

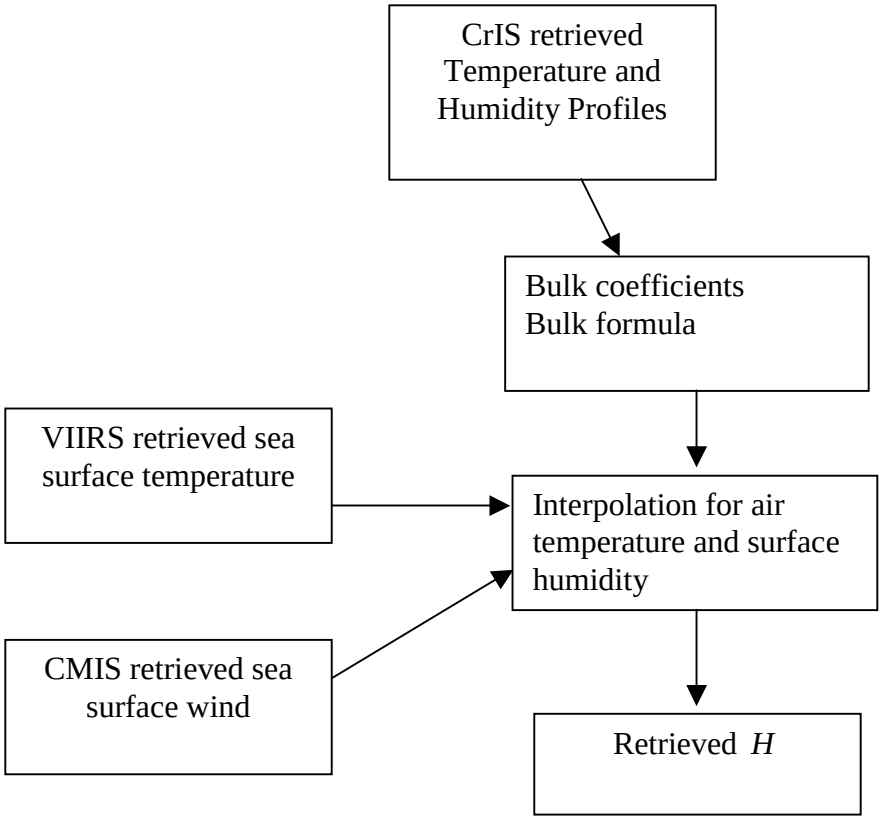

Figure 11. EDR flowdown process for sensible heat flux.

3.3 THEORETICAL DESCRIPTION OF NET HEAT FLUX RETRIEVALS

3.3.1 Physics of the Problem

The physics of Net Heat Flux is that of radiation processes and turbulence. There is no direct relation between satellite-measured radiance and the downward longwave and shortwave radiation (Fung *et al.,* 1984). Because satellite-borne sensors measure only the directional narrow–band radiance at the top of the atmosphere, the physics of retrieval of the surface radiation is composed of three parts: a) calculating downward narrow-band radiance at the surface by atmospheric correction for shortwave radiation or by statistical relation for longwave radiation; b) converting narrow-band radiance to broad-band radiance (0.2 – 4 μm for shortwave, 4 – 400 μm for longwave); and c) converting the directional broadband radiance to the angular integrated irradiance. Due to energy conservation, the shortwave net radiation at the

surface can be calculated from the solar incoming irradiance at the top of the atmosphere by extracting the reflected part at the TOA and the part absorbed by the atmosphere. The longwave net radiation over the ocean surface depends on the vertical structure of the temperature and humidity profile and sea surface temperature. VIIRS IR radiance is insufficient to take into account the vertical structure. At present, L_{net} is either calculated from the CrIS temperature and humidity profiles or from CMIS brightness temperatures. The CrIS calculation is based on the fact that a radiative transfer model can calculate radiation flux if the atmospheric state is known. The CMIS calculation is premised on the fact that satellite-measured brightness temperature contains the downward signal of the thermal radiation.

The latent and heat fluxes are turbulent energy, which is different from radiation energy. Both fluxes relate to satellite-measured radiances or brightness temperatures because they relate to the atmospheric state. The main weaknesses in the processes for determining latent and sensible heat fluxes rest in the validity of the bulk formula, the bulk coefficient, and air temperature and surface humidity.

3.3.2 Mathematical Description of the Algorithm

The retrieval algorithms for the four components of NHF are independent. Mathematical methods which may be used to derive each of the net heat flux components are described below.

3.3.2.1 Longwave Net Radiation Flux Calculated From CrIS Profiles and VIIRS SST/ IST

The method described here is the one implemented in the VIIRS Net Heat Flux Detailed Design *[Y-3230]*, that will be converted into operational code.

L_{net} can be calculated from a radiative transfer model if the atmospheric state is known. However, such computations are too expensive for operational satellites. According to an empirical formula developed by Gupta *et al*. (1992), L_{net} over the ocean surface can be expressed as:

$$L_{net} = \varepsilon_{IR}(F_d - \sigma T_s^4) \tag{8}$$

where σ is the Stefan-Boltzman constant, T_s is sea surface temperature. ε_{IR} is the longwave emissivity of the sea surface and its value is commonly assumed to be 0.98 (e.g. Gilman and Carret, 1994). The downward longwave radiation flux for a clear sky case is represented as:

$$F_d = (A_0 + A_1 V + A_2 V^2 + A_3 V^3) T_e^{3.7} \tag{9}$$

where $V = \ln W$, W is the total perceptible water, and T_e is an effective emitting temperature of the atmosphere. T_e is calculated as:

$$T_e = k_s T_s + k_1 T_1 + k_2 T_2 \tag{10}$$

The coefficients in (9) and (10) are as follows:

$$A_0 = 1.791\times10^{-7}, \quad A_1 = 2.093\times10^{-8}, \quad A_2 = -2.748\times10^{-9}, \quad A_3 = 1.184\times10^{-9}$$
$$k_s = 0.60, \qquad k_1 = 0.35, \qquad k_2 = 0.05$$

where T_1 and T_2 are the mean temperatures of the first and second atmospheric layers next to the surface. These layers cover the surface-800 mb, and 800-680 mb regions.

3.3.2.2 Longwave Net Radiation Flux Calculated From CMIS Brightness Temperature

This is an alternative method for deriving net longwave radiation fluxes, which is not currently implemented in the VIIRS prototype code. It requires the use of a neural network, which is described in Section 3.3.2.3. A neural network approach is also a possible method of deriving latent heat fluxes from CMIS brightness temperatures.

In the thermal infrared spectral range, scattering effects can be neglected for most applications. The scattering effects can also be neglected for non-precipitating and light-to-moderate raining clouds in the microwave spectrum at low frequencies. The equation describing the monochromatic radiative transfer through a plane-parallel atmosphere reads (Liou, 1980):

$$\mu \frac{dI(\delta,\mu)}{d\delta} = I(\delta,\mu) - B(T) \tag{11}$$

with I, the radiance, $\mu = \cos\theta$, θ the zenith angle, $B(T)$, the Planck function, T, the temperature, and δ, the optical depth. The solution of (11) at the top of the atmosphere can be written by (Simmer, 1994):

$$I_{IR} = \tau_{IR}\varepsilon_{IR}B(T_s) + I^u_{IR} + \tau_{IR}(1-\varepsilon_{IR})I^d_{IR} \tag{12}$$

in the thermal infrared spectral range, and:

$$TB_v = TB^u + \tau_{MW}\left[\varepsilon_v T_s + (1-\varepsilon_v)TB^d\right] \tag{13}$$

$$TB_h = TB^u + \tau_{MW}\left[\varepsilon_h T_s + (1-\varepsilon_h)TB^d\right] \tag{14}$$

in the microwave spectral range, where the radiance has been substituted by the brightness temperature using the Rayleigh-Jean's approximation. τ is the total transmittance of the atmosphere. The quantities I^u_{IR} and I^d_{IR} (TB^u and TB^d) are the upwelling and downwelling radiances (brightness temperatures). The subscripts *v* and *h* denote the vertical and the horizontal polarizations, respectively. ε_v and ε_h are the vertical and the horizontal components of the microwave sea surface emissivity, respectively.

The downward longwave radiation F^d_{IR} is calculated by:

$$F^d_{IR} = 2\pi\int_0^1 \mu I^d_{IR}\, d\mu \tag{15}$$

The downwelling radiance I_{IR}^{d} contributes very little to the measurements of satellite-based infrared radiometers because the thermal infrared emissivity of the sea surface ε_{IR} is close to one. This has been demonstrated by Ramanathan (1986), who compared the outgoing longwave radiative flux at the top of the atmosphere with the net longwave surface flux for selected regions from simulations with the NCAR general circulation model. The correlation between both fluxes is very poor. Because of the low microwave emissivity of the sea surface (about 0.5), microwave radiometers on satellites measure a mixed information containing contributions from the sea surface, the upwelling brightness temperature TB^{u}, and the downwelling brightness temperature TB^{d}. TB^{d} can be extracted by subtracting (14) from (13):

$$TB^{d} = T_{s} - \frac{TB_{v} - TB_{h}}{\tau_{MW}(\varepsilon_{v} - \varepsilon_{h})} \tag{16}$$

ε_{v} and ε_{h} are a function of the sea surface roughness caused by the wind and the sea surface temperature. The total transmittance of the atmosphere, τ_{MW}, is mainly a function of the total perceptible water (Stephens *et al.*, (1994), the cloud liquid water path and precipitation (Greenwald *et al.*, 1993; Petty, 1994; Weng and Grody, 1994; Wentz, 1992). The sea surface wind, sea surface temperature, total water vapor, cloud liquid path, and rain water can be determined from measurements of space-borne microwave radiometers (Goodberlet *et al.*, 1990; Crewell *et al.*, (1991; Bauer and Schluessel, 1992; Liu and Curry, 1992). Thus, with the polarization Q ($Q = TB_{v} - TB_{h}$) directly observable and all other parameters in (16) affecting microwave radiation, in general, information about TB^{d} is also contained in the microwave signal at satellite altitudes.

Table 5 shows the correlation coefficients between F_{IR}^{d} and TB^{d} for the four SSM/I frequencies. The downward longwave radiation and the downward brightness temperatures over oceanic areas are calculated with radiative transfer models from radiosonde data for 1989. In general, correlation coefficients for clear-sky cases are larger than for cloudy cases, especially at 37 GHz. The best correlation is found for clear-sky cases at 85 GHz because this channel shows the best relation to the boundary layer humidity, which dominates F_{IR}^{d}.

Table 5. Correlation coefficients between the downward longwave radiation and the downward brightness temperature at sea surface.

	19.35 GHz	22.235 GHz	37 GHz	85.5 GHz
all cases	0.81	0.90	0.59	0.82
clear-sky cases	0.95	0.95	0.95	0.97

To derive the algorithm, simultaneous values of the surface longwave radiation balance and passive microwave measurements from SSM/I are required. Such data do not exist. Therefore, simulated data are utilized instead. Because the developed method is statistical, the simulated

measurements are based on realistic atmospheric situations, which were obtained from ship-based radiosoundings. Clouds and precipitation are parameterized, and radiative transfer models are used to simulate the satellite radiances and surface longwave radiation balance.

From a global data set of about 10,000 ship-based radiosonde ascents for 1989 (Figure 1) was obtained from the German Weather Service (DWD), six months (January, March, May, July, September, November) were used as a training data set. The remaining six months are chosen as the validation set. Temperature and moisture profiles are interpolated to 40 layers. The top level of the interpolated profile is 40 km above the sea surface. The cloud liquid water profile is analyzed from the profiles using the modified adiabatic liquid water approach (Karstens *et al*, 1994). This method computes the adiabatic liquid water for contiguous layers with relative humidity above 95 percent. A height-dependent factor takes into account entertainment of dry air, precipitation, and freezing by scaling the liquid water profiles based on a parameterization obtained from aircraft measurements. It has been shown by Karstens *et al*. (1994) that this procedure produces realistic frequency distributions of total cloud liquid water contents and cloud-top heights.

Cloud ice is determined for cloudy layers with temperatures below -20°C according to the parameterization by Liou (1986). The parameterization is to fit the observed mean ice content as a function of temperature, based on the fact that temperature is the predominant factor controlling the ice crystal size and, as a consequence, the ice content.

The two-stream radiative transfer code by Schmetz (1986) is used to calculate the net sea surface longwave radiation. The two-stream code used is composed of 51 intervals covering a spectral range of from 4 to 400 μm. The two-stream approximation can achieve a quick approximate solution to the radiative transfer equation by decomposing the radiative field into two opposing streams (i.e., upward and downward streams). Although the microwave radiation polarization must be considered, it is beyond the capacity of the two-stream model.

The matrix operator method is one of the methods commonly used to account for the scattering and polarization. For a homogeneous layer, the matrix operator method solves the radiative transfer equation in analytical matrices. The solution of the radiative transfer equation for the vertically inhomogeneous atmosphere is obtained recurrently from the analytical solutions for a set of homogeneous layers, where the vertically inhomogeneous atmosphere is subdivided into a set of homogeneous layers. A matrix-operator radiative transfer code (Liu and Ruprecht, 1996) is used to calculate the seven brightness temperatures at the top of the atmosphere for the SSM/I frequencies (19.35 GHz, 37 GHz, 85.5 GHz both vertically and horizontally polarized; 22.235 GHz only vertically polarized).

The absorption coefficients of gases in the microwave spectrum are adopted from Liebe (1985). The parameterization of Wisler and Hollinger (1977) is used to model the reflection and emission of the sea surface in the microwave spectrum. For a given frequency the parameterization of Wisler and Hollinger (1977) needs the sea surface temperature and the

salinity to calculate the dielectric constant. The effects of the surface roughness and possible foam are parameterized as functions of the sea surface wind speed. Stability is not taken into account; thus, a single relation between wind speed and wind stress is assumed. In this study, salinity is set to 30 parts per 1,000 for all cases, because in the frequency range of SSM/I the effect of its variability is negligible.

3.3.2.3 Neural Network

An artificial neural network (Hertz *et al*., 1991) solves a problem arising from a highly connected array of elementary processors called neurons (Chen *et al*., 1995). Every elementary processor performs a simple function. A layered perception-type artificial neural network, which has one input layer, one or more hidden layers, and one output layer is used. Each layer employs several neurons, and each neuron in the same layer is connected to neurons in the adjacent layer with different weights (Tsang *et al*., 1992). The weights can be calculated from the back propagation-learning algorithm based on a training data set. This back propagation algorithm uses the gradient descent algorithm to get a local minimum between the calculated output and the actual output. To reduce the bias an additional neuron in the input layer and hidden layer with a fixed input value of one is introduced. The neural network algorithm may be described in the following steps:

1. Build a network containing appropriate neurons in one input layer, one or more hidden layers, and one output layer.

2. Scale input-output data, where the scaled values range between given minimum and maximum values of a sigmoid function.

3. Initialize the weights to small random values.

4. Choose an input-output pair (α_k, β_l) and apply it to the input layer ($m = 0$):

$$V_k^0 = \alpha_k \tag{1}$$

5. Propagate the input data forward through the network using:

$$V_i^m = g(h_i^m) = g(\sum_j w_{ji}^m V_j^{m-1}) \tag{2}$$

for each i and m until the final outputs V_i^M have all been calculated.

6. Compute the deltas (i.e., error) for the output layer:

$$\delta_i^M = g'(h_i^M)\left|\beta_i - V_i^M\right| \tag{3}$$

7. Compute the deltas for the preceding layers by propagating the errors backward:

$$\delta_i^{m-1} = g'(h_i^{m-1}) \sum_j w_{ji}^m \delta_j^m \tag{4}$$

for $m = M, M-1,...2,$ here g is a sigmoid function and g' is the derivation of the sigmoid function.

8. Use:

$$\Delta w_{ij}^{m} = \eta \delta_i^{m} V_j^{m-1} \tag{5}$$

to update the connection weights according to:

$$w_{ij}^{m}(new) = w_{ij}^{m}(old) + \Delta w_{ij}^{m} \tag{6}$$

9. Go back to step 4 for the next input-output pair until all input-output pairs propagate.

10. Repeat steps 4 through 9 until the maximum error (or rms error) between the calculated output and the actual output is smaller than the given error.

The sigmoid function can be any differential function. For this document we choose:

$$g(x) = \frac{1}{1+\exp(-x)} \tag{7}$$

3.3.2.4 Shortwave Radiation Flux

The downward shortwave radiation flux at the surface and top of the atmosphere can be calculated if the atmospheric state (e.g., surface reflectivity, aerosols, temperature, and humidity profiles) is known. The shortwave radiation flux can be calculated directly from VIIRS radiances for the proposed nine shortwave channels because the VIIRS measurements contain that atmospheric information, and the shortwave radiation flux is not sensitive to the vertical distribution of the temperature and moisture profiles. A regression algorithm is applied to calculate the downward shortwave radiation flux *SW* for given sun incidence and satellite viewing angles:

$$SW = a_0 + \sum_{k=1}^{10} a_k R_k \tag{17}$$

The regression coefficients, a_k, are determined by minimizing the root mean square error for the fixed sun incidence and satellite viewing angles. Equation (17) needs to be extended for the general cases. Then, the shortwave net flux can be derived:

$$Net\ SW = (1-\alpha)SW \tag{18}$$

and the surface albedo of the ocean (Hansen et. al., 1983) becomes:

$$\begin{aligned} \alpha &= 0.021 + 0.0421\,x^2 + 0.128\,x^3 - 0.04\,x^4 \\ &- \left[3.12/(5.68+WS) + (0.074x)/(1+3\,WS)\right] x^5 \end{aligned} \tag{19}$$

where $x = 1-\mu_0$, μ_0 is the cosine of the sun zenith angle and *WS* is the surface wind speed in units of m/s.

3.3.2.5 Sensible and Latent Heat Fluxes

Based on the eddy correlation approach, the sensible heat flux can be expressed as:

$$H = \rho c_p \left\langle w' \theta' \right\rangle \tag{20}$$

or

$$H = \rho c_p \left\langle w' T' \right\rangle \tag{21}$$

since near the surface $T' \approx \theta'$. Thus, in principle, the vertical fluxes can be evaluated from the direct measurements of the vertical velocity, w', and temperature. However, it is very difficult to obtain w', which prevents the use of this method. The sensible flux of heat can be written on the basis of the Prandtl assumption:

$$\begin{aligned} H &= \rho c_p \left\langle w' \theta' \right\rangle \\ &= -K_H \rho c_p \left\langle \frac{\partial \theta}{\partial z} \right\rangle \end{aligned} \tag{22}$$

where K_H is the eddy diffusion coefficient for heat. This equation implies that the vertical flux of heat is determined by the mean vertical potential temperature gradient. It also corresponds to the intuitive idea that heat flows from warm to cold levels proportionally to the gradient of the mean potential temperatures. Over the oceans, (21) can be approximately expressed by:

$$H = \rho c_p C_H (V - V_s)(T_s - T_A) \tag{23}$$

where C_H is the bulk coefficient, V is the sea surface wind speed at a reference height (e.g. 10m), T_s is the sea surface temperature, and T_A is the air temperature. V_s is the wind speed at the surface. c_p is the isobaric specific heat.

According to Fick's law, the net vertical flux of water vapor across the earth's surface is proportional to the specific humidity gradient (similar to sensible heat). The proportionality coefficient for the water vapor flux , α_w ,is the molecular diffusivity for water vapor:

$$E = -\rho \alpha_w \left\langle \frac{\partial q}{\partial z} \right\rangle \tag{24}$$

This expression is only valid in the laminar viscous sublayer, where molecular exchange is the prevalent transfer mechanism. The lower region of the surface boundary layer is almost always turbulent so that in this layer the water is transferred away from the molecular sublayer by turbulence. The vertical flux is then given by:

$$E = \rho c \left\langle w' q' \right\rangle \tag{25}$$

The transport in this mixed layer depends on surface roughness, wind shear, and thermal stratification. Therefore, the rate of transfer of water vapor (evaporation) depends on all these

factors as well as on the gradient of specific humidity. Then, a gradient-flux relation can be accepted and expressed in a bulk formula:

$$E = \rho L C_w (V - V_s)(q_s - q_A) \tag{26}$$

where L is the latent heat of vaporization. Its value is approximately $L = 2.456 \times 10^6\ Jkg^{-1}$. The mean q_s is generally assumed to be the saturation value at T_s. Air density can be calculated from near- surface pressure and temperature values using the ideal gas law, or approximated as $\rho = 1.15\ kgm^{-3}$.

For a simple case (i.e., neutral condition), the bulk coefficients are:

$c_p = 1005 Jkg^{-1}K^{-1}$ (Gilman and Carrett, 1994),

$C_w = 1.14 \times 10^{-3}$, $C_h = C_w / 1.2$

These values can be used as constants in a simplified version of the bulk transfer equations. However, for more accurate calculations, it should be taken into account that bulk coefficients for neutral conditions and unstable cases are different. Cold air blowing over warm water is heated from below and tends to convect. The air column becomes unstable, and the transfer of heat no longer depends solely on the turbulence generated by wind shear; rather, it is augmented with the turbulence generated by temperature instability.

The bulk coefficient for momentum is:

$$\tau = \rho C_D (V - V_s)^2 \tag{27}$$

where τ is the wind stress. Based on the surface-layer similarity theory, Liu *et al*. (1979) developed a bulk scheme with stability-dependent transfer coefficients. According to the theory, the mean diabatic profiles of V, θ and q, with a stability parameter $\xi = Z / L$ may be expressed as (e.g., Paulson, 1972):

$$(V - V_s)/u_* = [\ln(Z/Z_M) - \varphi_M(\xi)]/k_M \tag{28}$$

$$(\theta - \theta_s)/\theta_* = [\ln(Z/Z_M) - \varphi_H(\xi)]/k_H \tag{29}$$

$$(q - q_s)/q_* = [\ln(Z/Z_M) - \varphi_E(\xi)]/k_E \tag{30}$$

where the subscripts M, H, E indicate the quantities related to momentum, sensible heat and moisture, respectively. k_M, k_H, and k_E are various von Kármán constants, and are assigned 0.4, 0.45, and 0.45 by Liu *et al*. (1979), respectively. Z_M, Z_H, and Z_E are the various roughness lengths. The profile scaling parameters are given by:

$$u_* = (\tau/\rho)^{1/2} \tag{31}$$

$$\theta_* = -H/(\rho c_p u_*) \tag{32}$$

$$q_* = -E/(\rho L_v u_*) \tag{33}$$

The three stability functions, ϕ_M, ϕ_H, and ϕ_E, are related to the three dimensionless gradients, φ_M, φ_H, and φ_E, by the following expression:

$$\phi(\xi) = \int (1-\varphi) d \ln \xi \tag{34}$$

For unstable stratification, ϕ can be expressed as:

$$\phi_M = 2\ln\left[(1+(1-16\xi)^{1/4}/2\right] + \ln\left[(1+(1-16\xi)^{1/2}/2\right] - 2\tan^{-1}(1-16\xi)^{1/4} + \pi/2 \tag{35}$$

$$\phi_H = 2\ln\left[(1+(1-16\xi)^{1/4}/2\right] \tag{36}$$

$$\phi_E = 2\ln\left[(1+(1-16\xi)^{1/4}/2\right] \tag{37}$$

For the stable stratification, they are generally given as:

$$\phi_M = -7\xi \tag{38}$$

$$\phi_H = \phi_E = -7\xi \tag{39}$$

Including the effect of moisture on buoyancy, ξ can be defined as:

$$\xi = Zgk_M \theta_{v*}/(\theta_v u_*^2) \tag{40}$$

where g is the gravitational acceleration, θ_v is the virtual potential temperature, and:

$$\theta_{v*} = \theta_*(1+0.61q) + 0.61\theta q \tag{41}$$

The lower boundary parameters (Z_M, Z_H, and Z_E) are functions of τ and fluid properties. In order to have a gradual transition from smooth to rough flow, Z_M is assumed to be (Kondo, 1975):

$$Z_M = 0.0144 u_*^2/g + 0.11\nu/u_* \tag{42}$$

where ν is the kinematic viscosity of air. The values of Z_H and Z_E determined from the viscous interfacial-sublayer model of Liu *et al.* (1979) are given as functions of roughness Reynolds number $R_r = Z_M u_*/\nu$ as below:

$$Z_H u_*/\nu = a_1 (Z_M u_*/\nu)^{b_1} \tag{43}$$

$$Z_E u_*/\nu = a_2 (Z_M u_*/\nu)^{b_2} \tag{44}$$

where the values of a_1, a_2, b_1, b_2 for different ranges of R_r are given in Table 6 (adopted from Table 1 of Liu *et al*. [1979]).

Table 6. The lower boundary values of the logarithmic profiles.

R_r	a_1	b_1	a_2	b_2
0 - 0.11	0.177	0	0.292	0
0.11 - 0.825	1.376	0.929	1.808	0.826
0.825 - 3.0	1.026	-0.599	1.393	-0.528
3.0 - 10.0	1.625	-1.018	1.956	-0.870
10.0 - 30.0	4.661	-1.475	4.994	-1.297
30.0 - 100.0	34.904	-2.067	30.790	-1.845

With a suitable choice of von Kármán constants (k_M, k_H, and k_E) and unstable, dimensionless gradients (ϕ_M, ϕ_H, and ϕ_E), the three unknowns (τ, H, and E) can be determined by solving the three simultaneous equations 31-33 iteratively. The application of this model is similar to the use of a bulk aerodynamic scheme with variable transfer coefficients, which depend on atmospheric stability and surface roughness. The bulk coefficients can be expressed as:

$$C_D = k_M^2 / [\ln(Z / Z_M) - \phi_M(\xi)]^2 \quad (45)$$

$$C_H = C_D^{1/2} k_H^2 / [\ln(Z / Z_H) - \phi_H(\xi)]^2 \quad (46)$$

$$C_E = C_D^{1/2} k_E^2 / [\ln(Z / Z_E) - \phi_E(\xi)]^2 \quad (47)$$

3.3.3 Archived Algorithm Output

Net Heat Flux is a required EDR. All components of NHF (surface longwave net radiation, surface shortwave radiation, latent and sensible heat flux) and the outgoing longwave radiation flux as well as the outgoing shortwave radiation flux at the top of the atmosphere will also be produced because they are of great utility for different applications.

3.3.4 Variance and Uncertainty Estimates

The variations among the four components of Net Heat Flux are very large. Over oceans longwave net radiation can change from –50 Wm^{-2} to 150 Wm^{-2}. Shortwave net radiation flux varies from 0 Wm^{-2} to 1200 Wm^{-2}, sensible heat flux changes from –20 Wm^{-2} to 100 Wm^{-2}, and latent heat flux varies from –50 Wm^{-2} to 250 Wm^{-2}. The uncertainty estimate is 5-10 Wm^{-2} for longwave net radiation, 5-10 Wm^{-2} for the shortwave net radiation flux, 10-15 Wm^{-2} for sensible heat flux, and 20-25 Wm^{-2} for latent heat flux, based on simulation results.

3.3.4.1 Error budget

The error due to the VIIRS data on net heat flux EDR is small except for the surface albedo over ice. As an example, the error for the longwave radiation flux, $LWup$, in an upward direction can be exactly derived, where $LWup$ can be expressed as:

$$LWup = \varepsilon \, \sigma \, T_s^4 \tag{48}$$

The error for $LWup$ by sea surface temperature is:

$$\begin{aligned} \Delta LWup &= 4\varepsilon \, \sigma \, T_s^3 \, \Delta T_s \\ &= LWup \; 4 \, \frac{\Delta T_s}{T_s} \end{aligned} \tag{49}$$

For $T_s = 300K$, $\Delta T_s = 0.2K$, $\varepsilon = 1 \rightarrow \Delta LWup = 1.22 Watt/m^2$

By neglecting the uncertainty of the non-VIIRS data (for example, sea surface wind speed, air temperature, surface specific humidity and so on), threshold requirements for both precision and accuracy can be met for net heat flux over oceans (see Table 7). The threshold requirement for precision can be also met for net heat flux over ice, but the threshold requirements for accuracy is slightly failed due to the uncertainty of the surface albedo over ice (see Table 8).

The main error on net heat flux EDR is resulted from the uncertainty of non-VIIRS data. It fails to meet the threshold requirements for precision and accuracy when the uncertainty of non-VIIRS data is considered. The error budget is analyzed item-by-item (see Tables 9-10).

a. Forward model

MODTRAN 3.7 is used to calculate the long-wave net radiation flux at the surface. 6S is applied to calculate the short-wave radiation flux at the surface. It is generally believed that an error of 5 Wm^{-2} may exist in the measurements by using pyranometers for global radiation and pyrgeometers for the long-wave radiation flux. Thus, the 5 Wm^{-2} is chosen as an accuracy error in either forward model or in the measurement.

b. Atmospheric correction

A multiple regression method is used to calculate the downward short-wave radiation flux from VIIRS measurements. The calculation in the method is considered as an atmospheric correction error. The atmospheric correction error is 3.5 Wm^{-2}.

c. Sea surface wind speed

The sea surface wind speed is required for calculating the sensible and latent heat fluxes and the sea surface albedo required for the computation of net shortwave flux. The current SSM/I provides the global sea surface wind speed. The NPOESS CMIS instrument will provide both the sea surface wind speed and direction. The wind speed product of CMIS is required to have the accuracy of 1m/s or 10% of the true value, whichever is greater (NPOESS CMIS SRD objective requirement). The uncertainty of the sea surface wind speed can result in an error of approximately 8 Wm^{-2}. The wind direction is not considered in the bulk formula.

d. Temperature profile

The temperature profile is an important parameter for calculating the downward long-wave radiation flux at the surface. The uncertainty of the temperature profile is 1 K for the layer between the surface and 300 km (NPOESS CrIS SRD threshold requirement). The atmospheric effect on the downward long-wave radiation above 300 mb is small. The uncertainty of 1 K in the error budget has been adopted. The uncertainty of the temperature profile can result in an error of approximately 3 Wm^{-2}. For the short-wave radiation flux at the surface, it has little effect.

e. Humidity profile

The humidity profile is an important parameter for calculating the downward long-wave and the short-wave radiation fluxes at the surface. The uncertainty for the humidity profile is 15% for the layer between the surface and 600 mb (NPOESS CrIS SRD threshold requirement). This uncertainty has been adopted in the error budget. The uncertainty of the humidity profile can result in a total error of approximately 8 $Wm^{-2}$for the short-wave and long-wave radiation flux at the surface.

f. Air temperature

An uncertainty of 1 K for the air temperature is used. This is the same for the temperature profile. The air temperature effects the calculation of the sensible heat flux. The uncertainty of 1 K can result in an error of 6 Wm^{-2} for the net heat flux EDR.

g. Total column ozone

The total column ozone can be obtained from the operational product of OMPS, one of the NPOESS instruments. The ozone product is supposed to be better than 10 Dobson units (3 DU +/- 0.5%, NPOESS OMPS SRD). An uncertainty of 15 Dobson units is required. The error due to the uncertainty of the ozone amount is approximately 1 Wm^{-2}. The error in the ozone correction is used for all the error budget tables.

h. Surface specific humidity

The surface specific humidity is not available from NPOESS EDRs. It can be obtained by interpolating the humidity profile or from the surface temperature by assuming that the atmosphere just above the water or ice surface is saturated. The uncertainty of the surface specific humidity is too large compared to the VIIRS SRD requirement. Research results (Chou et al., 1995) have shown that the uncertainty is approximately 2g/kg. The latent heat flux can be derived directly from CMIS brightness temperatures. The latent heat flux error is approximately 20 $W/m2$ (Liu et al., 1999), which corresponds approximately to an uncertainty of 1 g/kg for the surface specific humidity.

i. Sea/ice surface temperature

The accuracy of 0.2 K for sea surface temperature can result in an error in the longwave, sensible, and latent heat fluxes of approximately 4.7 $W/m2$ because the surface temperature affects the long-wave net radiation flux at the surface and the sensible and latent heat fluxes. The

uncertainty of 0.3 K (RAYTHEON specified value) for ice surface temperature can result in an error approximately 4.9 Wm^{-2}.

j. Ice cover fraction

Near the water/ ice margin, an error in the estimate of ice cover fraction can result in an error

$$\Delta SW_{net} = \Delta f \cdot (\alpha_i - \alpha_w) \cdot SW_d$$

where ΔSW_{net} is the estimated error in the net downward shortwave flux, Δf is the error in the ice fraction, α_i is the albedo of ice, α_w is the albedo of water, and SW_d is the downward shortwave flux. Assuming values of 10% for Δf, 0.7 for a_i, 0.1 for a_w, and 200 W m^{-2} for SW_d yields a value of 12 W m^{-2} for ΔSWnet. This source of error will be highly variable, depending on the intensity of incoming shortwave radiation and ice albedo variation.

k. Absolute calibration

The surface short-wave radiation flux is almost proportional to the calibrated radiance. Comparisons of the radiation budget at the top of the atmosphere between the VIIRS derived and the other specific missions are very helpful. The calibration stability for the VIIRS bands is more important than the absolute calibration because the calculated shortwave radiation flux can be recalibrated by the surface measurement (there are some operational stations for the measurement). We use 0.5% accuracy for the recalibration based on the current accuracy of the surface measurements The 0.5% calibration error can result in an error of 4 Wm^{-2} for the net heat flux EDR over the oceans for downward short-wave radiation flux at surface of 800 Wm^{-2} and 1.5 Wm^{-2} for downward short-wave radiation flux over ice of 300 Wm^{-2} (monthly mean value in polar summer).

l. Radiometric noise

The net heat flux EDR is not sensitive to the VIIRS radiometric noise. The high signal-to-noise ratio of the ocean color bands is sufficient for this EDR. The noise is assumed to have a Gaussian distribution. The error in the calculation of the net heat flux EDR due to the radiometric noise is less than Wm^{-2} even without considering the aggregation of the pixels. The radiometric noise is negligible when one aggregates the VIIRS pixel into the 20 km by 20 km grid.

Table 7. Error budget for Net Heat Flux over oceans neglecting uncertainty of non-VIIRS data.

Net Heat Flux	Case: Global Ocean			(Standard atmospheric profile)
Specification v2 (Algorithm SFR)		Measurement		(9-bands) Unit: W/m^2
27-Oct-99	Accuracy	Precision	Uncertainty	Reference
Threshold	10.00	5.00	11.18	SRD Version 2, 1-Oct-99
Objective	1.00	1.00	1.41	SRD Version 2, 1-Oct-99
A-Specification	10.00	5.00	11.18	
Sensor B-Specification	4.00	2.00	4.47	
Algorithm B-Specification	6.88	2.00	7.16	
System Performance	7.95	2.83	8.44	
Algorithm Margin	0.00	0.00	0.00	
Algorithm Performance	6.88	2.00	7.16	RSS sum of algorithm errors
Forward Model	5.00	0.00	5.00	
Atmospheric Correction	0.00	2.00	2.00	
Sea Surface Wind Speed	0.00	0.00	0.00	<25 m/s
Temperature Profile	0.00	0.00	0.00	0%
Humidity Profile	0.00	0.00	0.00	0%
Air Temperature	0.00	0.00	0.00	0
Surface Specific Humidity	0.00	0.00	0.00	0 g/kg
Total Column Ozone	0.00	0.00	0.00	0 DU
Sea Surface Temperature	4.72	0.00	4.72	0.2 K
Sensor Performance	4.00	2.00	4.47	RSS sum of sensor errors
Absolute Calibration	4.00	0.00	4.00	0.5% for broadband shortwave radiation flux
Radiometric Noise	0.00	2.00	2.00	

Table 8. Error budget for Net Heat Flux over ice neglecting uncertainty of non-VIIRS data.

Net Heat Flux Specification v2 (Algorithm SFR) 27-Oct-99	Case: ice Accuracy	Measurement Precision	Uncertainty	(Standard atmospheric profile) (9-bands) Unit: W/m^2 Reference
Threshold	10.00	5.00	11.18	SRD Version 2, 1-Oct-99
Objective	1.00	1.00	1.41	SRD Version 2, 1-Oct-99
A-Specification	15.00	5.00	15.81	
Sensor B-Specification	1.50	2.00	2.50	
Algorithm B-Specification	11.41	2.00	11.58	
System Performance	11.51	2.83	11.85	
Algorithm Margin	0.00	0.00	0.00	
Algorithm Performance	11.41	2.00	11.58	RSS sum of algorithm errors
Forward Model	5.00	0.00	5.00	
Atmospheric Correction	0.00	2.00	2.00	
Surface Wind Speed	0.00	0.00	0.00	< 25 m/s
Temperature Profile	0.00	0.00	0.00	0 K
Humidity Profile	0.00	0.00	0.00	0%
Air Temperature	0.00	0.00	0.00	0 K
Surface Specific Humidity	0.00	0.00	0.00	0 g/kg
Total Column Ozone	0.00	0.00	0.00	0 DU
Ice Surface Albedo	9.00	0.00	9.00	3% Ref. RAYTHEON surface albedo
Ice Surface Temperature	4.92	0.00	4.92	0.3 K Raytheon specified uncertainty
Sensor Performance	1.50	2.00	2.50	RSS sum of sensor errors
Absolute Calibration	1.50	0.00	1.50	0.5% for broadband shortwave radiation flux
Radiometric Noise	0.00	2.00	2.00	

Table 9. Error budget for Net Heat Flux over oceans considering uncertainty of non-VIIRS data.

Net Heat Flux Specification v2 (Algorithm SFR) 27-Oct-99	Case: Global Ocean Measurement Accuracy	Precision	Uncertainty	(Ship-based Measured radiosondes) (9-bands) Unit: W/m^2 Reference
Threshold	10.00	5.00	11.18	SRD Version 2, 1-Oct-99
Objective	1.00	1.00	1.41	SRD Version 2, 1-Oct-99
A-Specification	10.00	25.00	26.93	
Sensor B-Specification	4.00	2.00	4.47	
Algorithm B-Specification	6.88	24.23	25.18	
System Performance	7.95	24.31	25.58	
Algorithm Margin	0.00	0.00	0.00	
Algorithm Performance	6.88	24.23	25.18	RSS sum of algorithm errors
Forward Model	5.00	0.00	5.00	
Atmospheric Correction	0.00	3.50	3.50	
Sea Surface Wind Speed	0.00	8.00	8.00	10% < 25 m/s
Temperature Profile	0.00	3.10	3.10	1 K
Humidity Profile	0.00	8.00	8.00	15%
Air Temperature	0.00	6.00	6.00	1 K
Total Column Ozone	0.00	1.00	1.00	10 DU
Surface Specific Humidity	0.00	20.00	20.00	2 g/kg
Sea Surface Temperature	4.72	0.00	4.72	0.2 K
Sensor Performance	4.00	2.00	4.47	RSS sum of sensor errors
Absolute Calibration	4.00	0.00	4.00	0.5% for broadband shortwave radiation flux
Radiometric Noise	0.00	2.00	2.00	

Table 10. Error budget for Net Heat Flux over ice considering uncertainty of non-VIIRS data.

Net Heat Flux Specification v2 (Algorithm SFR) 27-Oct-99	Case: ice Accuracy	Measurement Precision	Uncertainty	(Ship-based Measured radiosondes) (9-bands) Unit: W/m^2 Reference	
Threshold	10.00	5.00	11.18	SRD Version 2, 1-Oct-99	
Objective	1.00	1.00	1.41	SRD Version 2, 1-Oct-99	
A-Specification	15.00	25.00	26.93		
Sensor B-Specification	9.74	6.81	4.02		
Algorithm B-Specification	11.41	24.05	26.62		
System Performance	11.51	24.14	26.74		
Algorithm Margin	0.00	0.00	0.00		
Algorithm Performance	11.41	24.05	26.62	RSS sum of algorithm errors	
Forward Model	5.00	0.00	5.00		
Atmospheric Correction	0.00	2.00	2.00		
Surface Wind Speed	0.00	8.00	8.00	10%	< 25 m/s
Temperature Profile	0.00	3.10	3.10	1 K	
Humidity Profile	0.00	8.00	8.00	15%	
Air Temperature	0.00	6.00	6.00	1 K	
Surface Specific Humidity	0.00	20.00	20.00	2 g/kg	
Total Column Ozone	0.00	1.00	1.00	10 DU	
Ice Surface Albedo	9.00	0.00	9.00	3%	
Ice Surface Temperature	4.92	0.00	4.92	0.3 K	Raytheon specified uncertainty
Sensor Performance	1.50	2.00	2.50	RSS sum of sensor errors	
Absolute Calibration	1.50	0.00	1.50	0.5% for broadband shortwave radiation flux	
Radiometric Noise	0.00	2.00	2.00		

The large uncertainties for the latent and sensible heat fluxes relate to the air temperature and surface specific humidity even if the objective requirement for the atmospheric temperature and humidity profiles can be achieved. This point can be directly seen from the bulk formula. A ten percent error in the sea surface wind results in an error of 10 Wm^{-2} for the latent heat flux and an error of 3 Wm^{-2} for the sensible heat flux. A ten percent error in surface humidity results in errors of 15 Wm^{-2} and 8.4 Wm^{-2} for the latent and sensible heat fluxes, respectively.

The estimate of the total error for NHF EDR is about 30 Wm^{-2}. The primary goal for the Net Heat Flux EDR is to achieve an uncertainty of 20-25 Wm^{-2}.

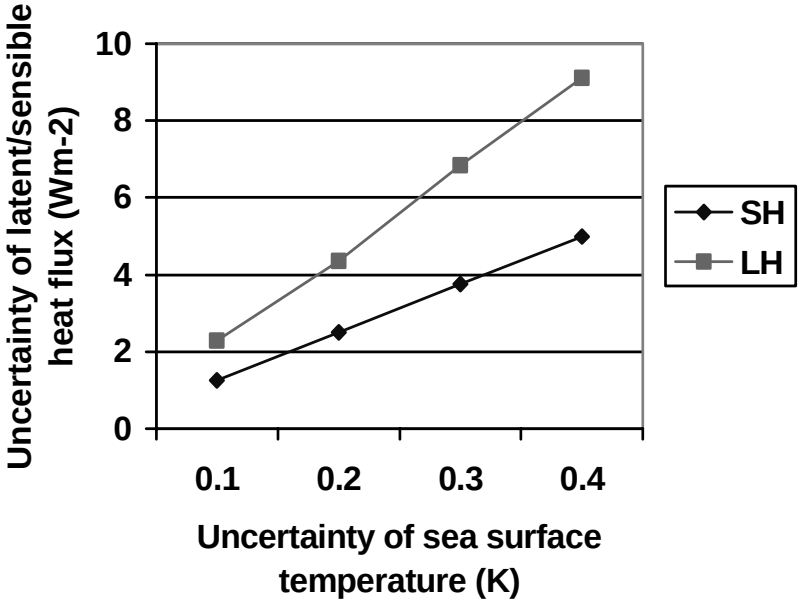

Figure 12. Sensitivity test for the latent and sensible heat fluxes with the uncertainty of the sea surface temperature.

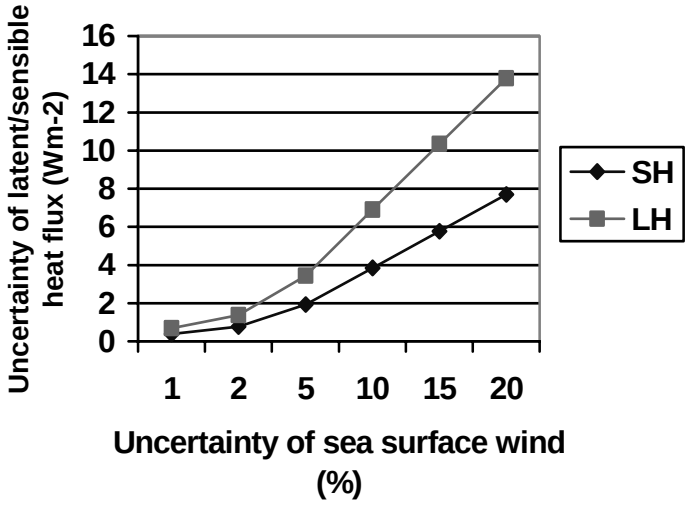

Figure 13. Sensitivity test for the latent and sensible heat fluxes with the uncertainty of the sea surface wind.

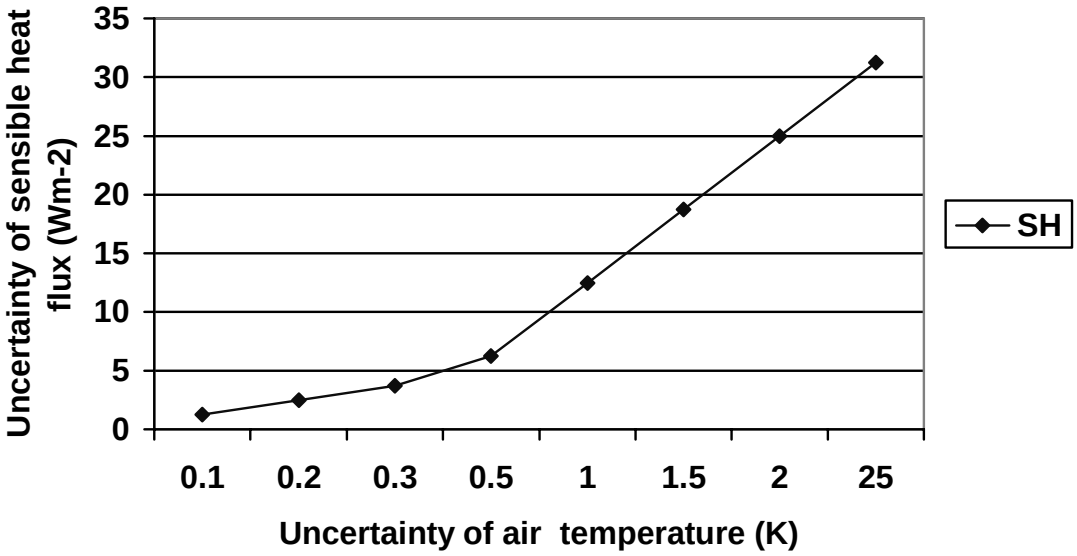

Figure 14. Sensitivity test for the latent and sensible heat fluxes with the uncertainty of air temperature.

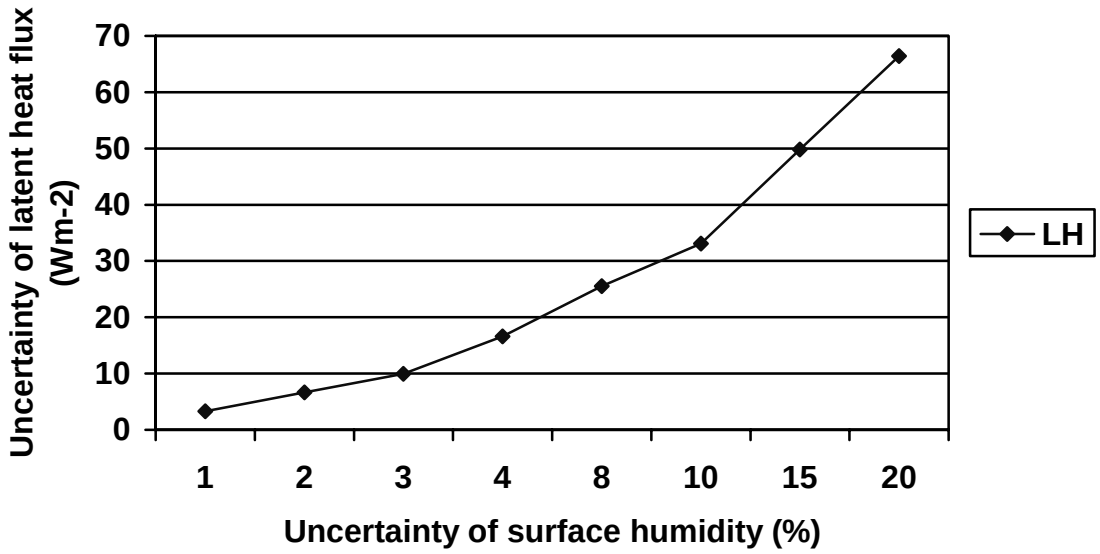

Figure 15. Sensitivity test for the latent and sensible heat fluxes with the uncertainty of surface humidity.

3.4 ALGORITHM SENSITIVITY STUDIES

As shown in Figure 6, the downwelling shortwave radiation flux at the surface can be determined directly from VIIRS radiances. The longwave net radiation flux over oceans can be derived from CrIS profiles and VIIRS SSTs. Both derived shortwave and longwave radiation fluxes meet the NPOESS threshold requirements. Expected uncertainties in air temperature and surface-specific humidity are too high for retrieved latent and sensible heat fluxes to satisfy the threshold value

for precision. The precision objective for the CrIS air temperature EDR is no better than 0.5 K, and the precision objective for the CrIS surface specific humidity is no better than ten percent. This can be seen from the following bulk formula for the neutral condition:

$$H = \rho C_p C_h U_{10}(T_s - T_a) \approx U_{10}(T_s - T_a) \quad (50)$$

$$E = \rho C_e L U_{10}(q_s - q_a) \approx 3.5\, U_{10}\,(q_s - q_a) \quad (51)$$

Thus, the retrieval error can be simulated from radiosondes (Figure 7). The lower right panel indicates that, for the sea surface wind of 10 ms^{-1}, a 10 percent error in the specific humidity of the air results in an error of 35 Wm^{-2} in calculating the latent heat flux E. A measurement uncertainty of 20 – 25 Wm^{-2} from the CMIS radiance has been obtained at the present. The retrieval accuracy needs to be further improved.

3.4.1 Calibration Errors

The calibration request from the Net Heat Flux EDR is too high to be satisfied. A one percent calibration error in the shortwave region can cause an error of 10 Wm^{-2}. Therefore, the retrieved radiation fluxes over oceans need to be compared and adjusted with ground truth measurements, which can be obtained from BSRN (Baseline Surface Radiation Network). BSRN is a project of the World Climate Research Program (WCRP), aimed at detecting important changes in the earth's radiation field, which may cause climate changes. At a small number of stations (fewer than 40) in contrasting climate zones, covering a latitude range from 80°N to 90°S, solar and atmospheric radiation is measured with instruments of the highest available accuracy and at a very high frequency (minutes).

3.4.2 Instrument Noise

Only one of the four components—the shortwave radiation flux over the ocean surface—depends directly on the sensor noise. It can be seen from Figure 6 that sensor model 3 or better can satisfy the EDR requirement for precision.

3.4.3 Other

The VIIRS Net Heat Flux EDR is strongly dependent on the retrieval accuracy of other EDRs from VIIRS and other instruments (CrIS and CMIS). Sea surface temperature is required to have an accuracy of 0.1 K. Uncertainties of low- level air temperature and surface specific humidity need to be better than 0.4 K and one percent, respectively. Uncertainties in the atmospheric temperature and humidity profiles are required to better than 0.5 K and ten percent, respectively. Retrieval error of the sea surface wind needs to be better than five percent.

3.5 PRACTICAL CONSIDERATIONS

Absolute calibration error of less than one percent in visible channels is not realistic. This difficulty may be overcome by adjustment according to ground truth measurements. Retrieval

error of 0.5 K and ten percent for atmospheric temperature and humidity may be achieved in the future. Retrieval error of the sea surface temperature is approximately 0.5 K on a scale of kilometers. The retrieval error could be expected to be about 0.1 K on a spatial resolution of 20 km in the future. It is possible to obtain a retrieval error of five percent for the sea surface wind in the future. However, it is very difficult to achieve accuracy within 0.4 K and 1 percent for low- level air temperature and surface-specific humidity.

3.5.1 Numerical Computation Considerations

Algorithms will be optimized for retrieving the difference between SST and air temperature and for the difference between humidity at skin and humidity at ten meters above the skin.

3.5.2 Programming and Procedural Considerations

The uncertainty of the sea surface temperature derived from the VIIRS instrument is better than 0.5 K for a spatial resolution of about 1.3 km. For a spatial resolution of 20 km, a threshold requirement of the Net Heat Flux EDR, a better precision of 0.3 K for the sea surface temperature can be expected. Combining the VIIRS data and CrIS data, an optimal retrieval algorithm for the boundary layer is under development. All codes will be written in FORTRAN.

3.5.3 Configuration of Retrievals

The configuration of the retrieval for the Net Heat Flux is separated into parts: radiation fluxes and turbulent fluxes. Shortwave net radiation at the surface will be calculated from VIIRS radiances at shortwave range based on a regression method. The shortwave net radiation flux can be obtained from the VIIRS aerosol optical depth and CrIS atmospheric temperature and humidity profiles products, as well as from the total ozone amount by an empirical formula (Darnell *et al*., 1992). The longwave net radiation flux can be calculated from the atmospheric temperature and humidity profiles and sea or ice surface temperature by applying an empirical formula (Gupta *et al*., 1992). A retrieval package for the boundary layer has been developed for calculating the low- level air temperature and surface specific humidity from VIIRS and CrIS data. [Bulk coefficients will be calculated from the boundary parameters: air temperature, sea surface temperature, surface specific humidity, and sea surface wind.]

3.5.4 Quality Assessment and Diagnostics

Because the Net Heat Flux is for the clear sky cases only, the local variation of the shortwave net radiation flux over oceans should be relatively small. The monthly mean value of the shortwave net radiation fluxes must be checked against the ground truth to allow calibration. Any large jump of ten percent (daily) to a previous day will be automatically checked to verify whether the large jump is due to volcanic ash or a calibration error. The variation of the longwave net radiation flux and the latent and sensible heat fluxes can be large in the vicinity of a warm or cold front.

3.5.5 Exception Handling

If CMIS is not available, the sea surface wind speed from SSM/I or analysis from a numerical model such as NCEP will be used. Atmospheric profiles of temperature and humidity are also required from an analysis if both CMIS and CrIS are not available.

3.6 ALGORITHM VALIDATION

The algorithm validation will be performed in two ways: model simulations and comparisons with other data sets, for example, ground measurements and other satellite measurements such as CERES (Clouds and the Earth's Radiation Energy System). Simulations will be performed using the commonly applied radiative transfer codes and the radiosonde measurements. It is found the VIIRS radiances for the sensor model 3 or better can be used to determine the shortwave net radiation flux over the oceans (see Figure 6). [The surface longwave net radiation (Liu *et al*., (1997) can be obtained from CMIS microwave flux (see Figure 16).] The radiation fluxes at the top of the atmosphere can be derived from VIIRS radiances (see Figure 7). The CrIS derived atmospheric profiles and VIIRS aerosol optical depth can be applied to calculate the radiation flux at the top of the atmosphere. A fast algorithm for calculating the downward longwave flux from the atmospheric profile is developed and tested. The algorithm is based on the results of EOF analysis. Figure 17 shows very good agreement between the results from detailed MODTRAN radiative transfer calculation and the present retrieval. One can compare the results with the measured fluxes at the top of the atmosphere from CERES to recalibrate the surface radiation fluxes of VIIRS. The turbulent energy can be checked with ground truths. Air temperature and surface humidity as well as sea surface wind can be compared with the values from a numerical prediction model or from an analysis of the field.

3.7 ALGORITHM DEVELOPMENT SCHEDULE

An algorithm for calculating downward surface shortwave radiation flux from VIIRS measurements has been developed. The algorithms for calculating longwave net flux at surface and latent and sensible heat fluxes from the atmospheric profile have also been developed. However, the results do not meet SRD requirement for precision when ancillary data error is considered. Direct calculation of the latent and sensible heat fluxes from CMIS data is under development because each component can be derived from microwave measurements.

The downward short-wave radiation flux over oceans can be calculated accurately from VIIRS radiance (see Figure 18). For a given surface albedo of ice, the short-wave net radiation flux over ice also can be derived from VIIRS radiance (see Figure 19).

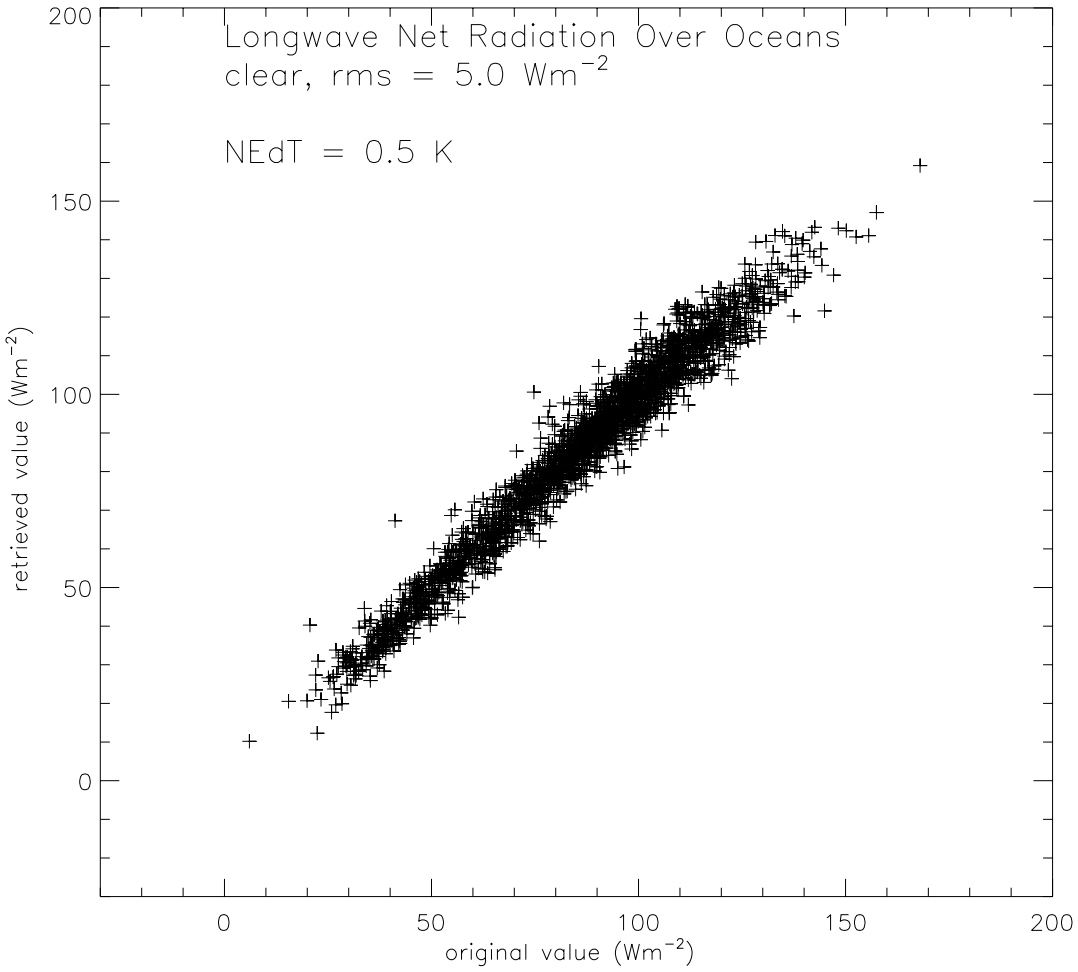

Figure 16. Comparisons of the original and CMIS brightness temperature retrieved longwave net radiation flux over the oceans.

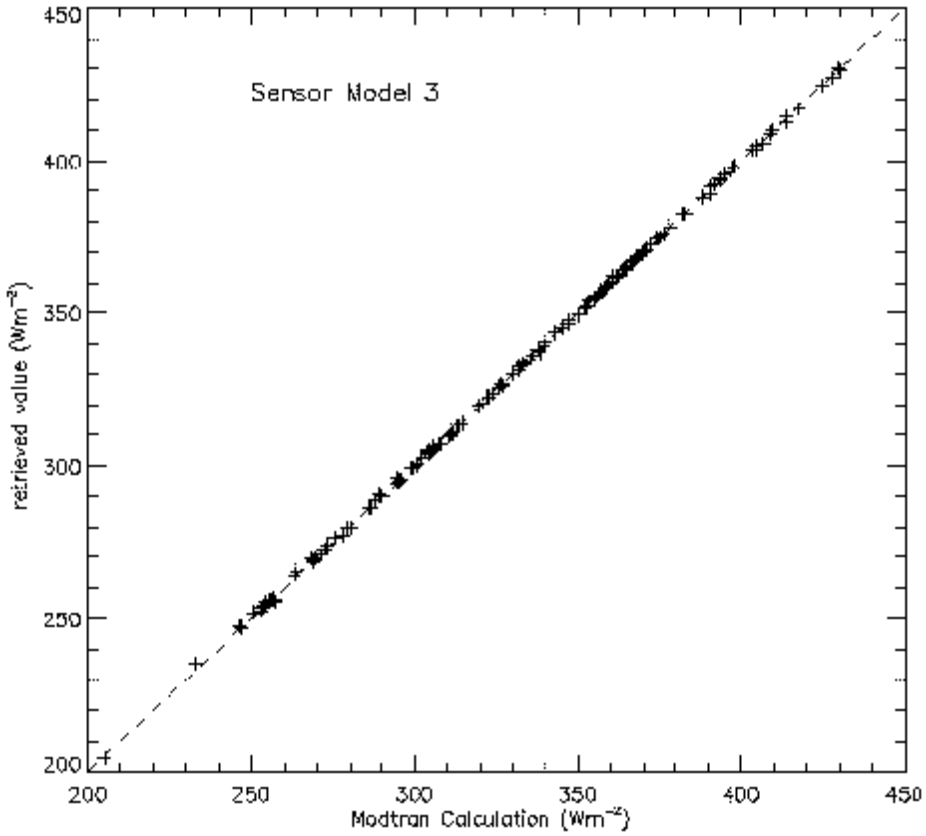

Figure 17. Comparisons of the downward surface longwave flux over the ocean between detailed MODTRAN calculations and present retrieval.

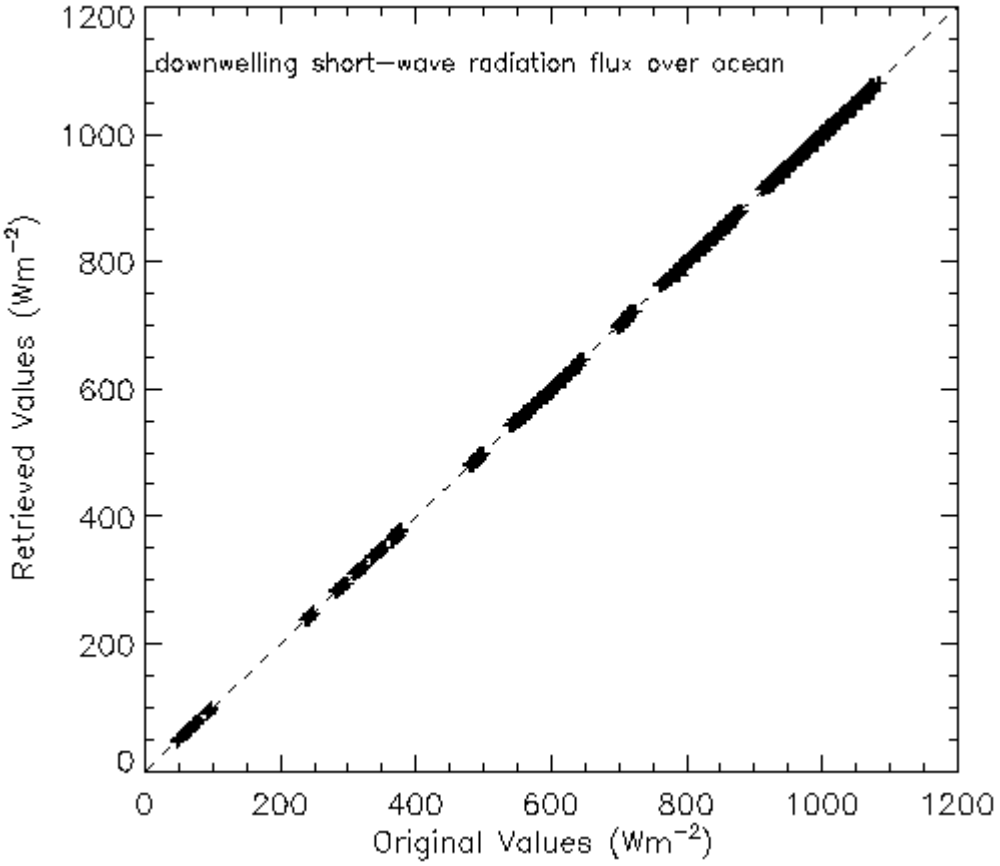

Figure 18. Comparisons of original and VIIRS radiance retrieved short-wave net radiation flux over the oceans.

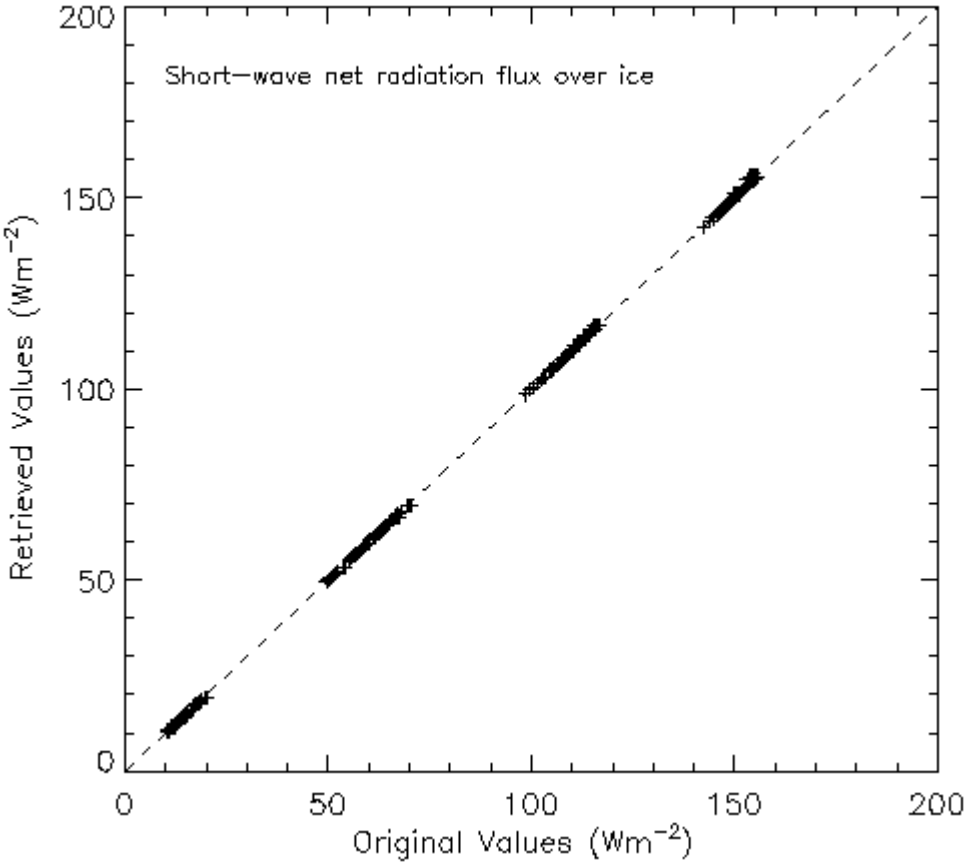

Figure 19. Comparisons of original and VIIRS radiance retrieved short-wave net radiation flux over ice.

4.0 ASSUMPTIONS AND LIMITATIONS

4.1 ASSUMPTIONS

The radiative transfer code MODTRAN is assumed to be within an accuracy of 5 Wm^{-2} for the calculation of the surface radiation fluxes.

4.2 LIMITATIONS

Retrievals are limited to conditions where the sea surface wind is below 25 ms^{-1}.

In order to meet the threshold requirement for the precision of 5 Wm^{-2} the total uncertainty for both the sea surface temperature and air temperature must be less than 0.2 K. The uncertainty for surface specific humidity needs to be smaller than two percent. Presently, such high requirements for the air temperature and surface specific humidity should not be expected. CMIS radiances and its EDR sea surface wind also are required.

5.0 REFERENCES

5.1 VIIRS DOCUMENTS

[Y-1] Visible/Infrared Imager/Radiometer Suite (VIIRS) Sensor Requirements Document (SRD) for National Polar-orbiting Operational Environmental Satellite System (NPOESS) Spacecraft and Sensors, Version 2, November 1999.

[Y-3230] Visible/Infrared Imager/Radiometer Suite (VIIRS) Net Heat Flux Unit Level Detailed Design, Version 4, January 2002.

5.2 NON-VIIRS DOCUMENTS

Agee, E. M., and R. P. Howley (1977). Latent and sensible heat flux calculations at the air-sea interface during AMTEX 74, *J. Appl. Meteor*., 16, 443-447.

Anderson, E. R.(1952). Energy budget studies. *U.S. Geol. Surv. Circ*., 229, 71-119.

Bauer, P., and P. Schluessel (1993). Rainfall, Total Water, Ice Water, and Water Vapor Over Sea From Polarized Microwave Simulations and Special Sensor Microwave/Imager Data.

Blanc, T. V. (1987). Accuracy of bulk method determined flux, stability, and roughness, *J. Geophys. Res*., 29, 3867-3876.

Brutsaert, W. (1982). *Evaporation into the Atmosphere*. Kluwer, Dordrecht, Holland: Boston: Reidel: Hingham, MA., 299pp.

Budyko, M. I. (1974). Climate and Life. *Int. Geophys. Ser*., Vol. 18, Academic Press, London, 508 pp.

Chen, K. S., W. L. Kao, and Y. C. Tzeng (1995). Retrieval of surface parameters using dynamic learning neural network. *Int. J. Remote Sensing*, 16, 801-809.

Chou, S.-H. (1993). A comparison of airborne eddy correlation and bulk aerodynamic methods for ocean-air turbulent fluxes during cold-air outbreaks. *Bound.-Layer Meteor*., 64, 75-100.

Chou, S.-H., R. M. Atlas, C. L. Shie, J. Ardizzone (1995). Estimates of surface humidity and latent heat fluxes over oceans from SSM/I data, *Monthly Weather Review*, 123, 2405-2425.

Crewell, S., E. Ruprecht, and C. Simmer (1991). Latent Heat Flux Over the North Atlantic Ocean - A Case Study. *J. Appl. Meteorol*., 30, 1627-1635.

Curry J. A., C. A. Clayson, W. B. Rossow, R. Reeder, Y.-C. Zhang, P. J. Webster, G. Liu, and R.-S. Sheu, 1999: High-Resolution Satellite-Derived Dataset of the Surface Fluxes of

Heat, Freshwater, and Momentum for the TOGA COARE IOP. *Bull. Ame. Meteorol. Soc*., 80, 2059-2080.

Darnell, W. L., W. F. Staylor, S. K. Gupta, N. A. Ritchey, and A. C. Wilber (1992). Seasonal variation of surface radiation budget derived from International Satellite Cloud Climatology Project C1 data. *J. Geophys. Res*., 97, 15741-15760.

Darnell, W. L., and W. F. Staylor (1988). Estimation of surface insolation using sun-synchronous satellite data. *J. Climate*, 1, 820-835.

Fung, I. Y., D. E. Harrison, and A. A. Lacis. (1984). On the variability of the net longwave radiation at the ocean surface. *Rev. Geophys*., 22, 177-193.

Garratt, J. R. (1977). Review of drag coefficients over oceans and continents. *Mon. Wea. Rev*., 105, 915-929.

Gilman, C. and C. Carrett (1994). Heat flux parameterizations for the Mediterranean Sea: The role of atmospheric aerosols and constraints from the water budget. *J. Geophys. Res*., 99, 5119-5134.

Goodberlet, M. A., C. I. Swift, and I. C. Wilheon (1990). Ocean surface wind speed measurements of the special microwave imager (SSM/I). *IEEE Trans. Geosci. Remote Sensing*, GE-28, 823-827.

Greenwald, T., G. L. Stephens, T. H. Vonder Haar, and D. L. Jackson (1993). A Physical Retrieval of Cloud Liquid Water Over the Global Oceans Using Special Sensor Microwave/Imager (SSM/I) observations. *J. Geophys. Res*., 98, 18471-18488.

Gupta, S. K. (1989). A parameterization for longwave surface radiation from sun-synchronous satellite data, *J. Climate*, 2, 305-320.

Gupta, S. K., W. L. Darnell, and A. C. Wilber (1992). A parameterization for longwave surface radiation from satellite data – Recent improvements, *J. Appl. Meteorol*., 31, 12, 1361-1367.

Haferman, J. L., E. N. Anagnostou, D. Tsintikidis, W. F. Krajewski, and T. F. Smith (1996). Physical based satellite retrieval of precipitation using a 3 D passive microwave radiative transfer model. *J. Atmos. Oceanic Technol*., 13, 832-850.

Hansen, J. E., G. Russel, D. Rind, P. Stone, A. Lacis, L. Travis, S. Lebedeff, and R. Ruedy, (1983). Efficient three-dimensional global models for climate studies: Model I and II. *Mon. Wea. Rev.*, 111, 609-662.

Harris, A. R., S. J. Brown, and I. M. Mason (1994). The effect of wind speed on sea surface temperature retrieval from space. *Geophy. Res. Lett*., 21, 1715-1718.

Hennings, D., M. Quante, and R. Sefzig (1990). International Cirrus Experiment 1989 Field Phase Report. *Institute of Geophysics und Meteorology*, University of Köln, F. R. Germany, 129 pp.

Hertz, J., A. Krogh, and R. G. Palmer (1991). Introduction to the Theory of Neural Computation. Addison-Wesley Publishing Company, 327 pp.

Isemer, H-J. and L. Hasse (1985). The Bunker Climate Atlas of the North Atlantic Ocean. Vol. 1, *Observations*. Spinger Verlag, Berlin, 218 pp.

Karstens, U., C. Simmer, and E. Ruprecht (1994). Remote sensing of cloud liquid water. *Meteorol. Atmosph. Phys*., 54, 157-171.

Kondo, J. (1975). Air-sea bulk transfer coefficients in adiabatic conditions. *Boundary Layer Meteorol*., 9, 91-112.

Large, W. G., and S. Pond (1981). Open ocean momentum flux measurements in moderate to strong winds, *J. Phys. Oceanogr*., 12, 464-482.

Li, Z., H. G. Leighton, and R. D. Cess (1993). Surface net solar radiation estimated from satellite measurements – comparisons with tower observations. *J. Climate*, 6, 1764-1772.

Liebe, H. J. (1985). An updated model for millimeter wave propagation in moist air. *Radio Science*, 20, 1069-1089.

Liou, K. N. (1980). An Introduction to Atmospheric Radiation. Academic Press, New York, 392 pp.

Liou, K. N. (1986). Influence of cirrus clouds on weather and climate processes: A global perspective. *Mon. Wea. Rev*., 114, 1167-1199.

Liu, G., and J. A. Curry (1992). Retrieval of precipitation from satellite microwave measurement using both emission and scattering. *J. Geophys. Res*., 97, 9959-9974.

Liu, Q., and E. Ruprecht (1996). A radiative transfer model: matrix operator method. *Appli. Opt*., 35, 4229-4237.

Liu, Q., C. Simmer, and E. Ruprecht (1997). Estimating longwave net radiation at sea surface from the special sensor microwave/imager (SSM/I). *J. Appl. Meteorol*., 36, 919-930.

Liu, W. T., K. B. Katsaros, and J. A. Businger (1979). Bulk parameterization of air-sea exchanges of heat and water vapor including the molecular constraints at the surface. *J. Atmos. Sci*., 36, 1722-1735.

Liu, W. T. and A. Zhang (1994). Evaporation and solar irradiance as regulators of sea surface temperature in annual and interannual change. *J. Geophys. Res*., 99, 12623-12637.

Paulson, C. A., E. Leavitt, and R. G. Fleagle (1972). Air-sea transfer of momentum, heat and water determined from profile measurements during BOMEX. *J. Phys. Oceanogr*., 2, 487-497.

Petty, G. W. (1994). Physical retrievals of over-ocean rain rate from multichannel microwave imagery. Part II: Algorithm implementation. *Meteorol. Atmos. Phys*., 54, 101-122.

Priestley, C. H. B. (1966). The limitation of temperature by evaporation in hot climate. *Agric. Meteorol*., 3, 241-246.

Ramanathan, V. (1986). Scientific use of surface radiation budget data for climate studies. Position paper in NASA RP-1169.

Ramanathan, V. and W. Collins (1991). Thermodynamics regulation of ocean warming by cirrus clouds deduced from observations of 1987 El Nino. *Nature*, 351, 27-32.

Robinson, I. S., N. C. Wells, and H. Chamoch (1984). The sea surface thermal boundary layer and its relevance to measurement of sea surface temperature by air-borne and space-borne radiometers. *Int. J. Rem. Sens*., 5, 19-45.

Schluessel, P. (1996). Satellite remote sensing of evaporation over sea. NATO ASI Series, Vol. 45, Radiation and water in the climate system: 431-461.

Schmetz, J. (1986). An atmospheric-correction scheme for operational application to METEOSAT infrared measurements. *ESA*, 10, 145-159.

Schmetz, J. (1989). Towards a surface radiation climatology: Retrieval of downward irradiances from satellites. *Atmospheric Research*, 23, 287-321.

Simmer, C. (1994). Satellitenfernerkundung Hydrologischer Parameter der Atmosphäre mit Mikrowellen. Verlag, Dr. Kovac, 313 pp.

Smith, W. L. and H. M. Woolf (1983). Geostationary satellite sounder (VAS) observations of longwave radiation flux. Paper presented at the: Satellite Systems to Measure Radiation Budget Parameters and Climate Change Signal. International Radiation Commission, Igls, Austria, 29, Aug.–2 Sep.

Stephens, G. L., D. L. Jackson, and J. J. Bates (1994). A Comparison of SSM/I and TOVS Column Water Data over the Global Oceans. *Meteorol. Atmos. Phys*. 54, 183-201.

Tsang, L., Z. X. Chen, Seho Oh, R. J. Marks, and A. T. C. Chang (1992). Inversion of Snow Parameters from Passive Microwave Remote Sensing Measurements by a Neural Network Trained with a Multiple Scattering Model. *IEEE Trans. Geosci. and Remote Sensing*, 30, 1015-1024.

Vermote, E. F., J. L. Deuze′, M. Herman, and J. J. Morcrette (1997). Second simulation of the satellite signal in the solar spectrum GS: Overview. *IEEE Trans. Geosci. and Remote Sensing*, 35, 675-686.

Visible/Infrared Imager/Radiometer Suite (VIIRS), Sensor Requirements Document (SRD) for National Polar-orbiting Operational Environmental Satellite System (NPOESS) Spacecraft and Sensors, Integrated Program Office, page 34 (1997) [document is available from http://www.laafb.af.mil/SMC/PK/NPOESS].

Weng, F. Z. and N. Grody (1994). Retrieval of cloud water using the special sensor microwave imager (SSM/I). *J. Geophys. Res*., 99, 25535-25551.

Wentz, F. J. (1992). Measurement of Oceanic Wind Vector Using Satellite Microwave Radiometers. *IEEE Trans. Geosci. and Remote Sensing*, 30, 960-972.

Wisler, M. M. and J. P. Hollinger (1977). Estimation of marine environmental parameters using microwave radiometric remote sensing systems. N.R.L. Memo. Rept. 3661, pp 27.

Zhi, H. and Harshvardhan (1993). A Hybrid Technique for Computing the Monthly Mean Net Longwave Surface Radiation over Oceanic Areas. *Theor. Appl. Climatol*. 47, 65-79.